EFFECTS OF ELASTIC EDGE RESTRAINTS AND INITIAL PRESTRESS ON THE BUCKLING RESPONSE OF COMPRESSION-LOADED COMPOSITE PANELS

Mark W. Hilburger[*], Michael P. Nemeth[†], Jaret C. Riddick[‡], Robert P. Thornburgh[§]
Mechanics and Durability Branch
NASA Langley Research Center
Hampton, Virginia 23681-0001

Abstract

A parametric study of the effects of test-fixture-induced initial prestress and elastic edge restraints on the prebuckling and buckling responses of a compression-loaded, quasi-isotropic curved panel is presented. The numerical results were obtained by using a geometrically nonlinear finite element analysis code with high-fidelity models. The results presented show that a wide range of prebuckling and buckling behavior can be obtained by varying parameters that represent circumferential loaded-edge restraint and rotational unloaded-edge restraint provided by a test fixture and that represent the mismatch in specimen and test-fixture radii of curvature. For a certain range of parameters, the panels exhibit substantial nonlinear prebuckling deformations that yield buckling loads nearly twice the corresponding buckling load predicted by a traditional linear bifurcation buckling analysis for shallow curved panels. In contrast, the results show another range of parameters exist for which the nonlinear prebuckling deformations either do not exist or are relatively benign, and the panels exhibit buckling loads that are nearly equal to the corresponding linear bifurcation buckling load. Overall, the results should also be of particular interest to scientists, engineers, and designers involved in simulating flight-hardware boundary conditions in structural verification and certification tests, involved in validating structural analysis tools, and interested in tailoring buckling performance.

Introduction

Curved panels are a common structural element found in many aerospace vehicles. With the need to reduce structural weight of aircraft and to exploit stiffness tailoring of fiber-reinforced, laminated-composite materials to enhance performance, there has come the need to understand the behavioral characteristics of thin-walled curved panels that may possess high degrees of material orthotropy and anisotropy. Orthotropy and anisotropy are manifested physically by couplings between deformation modes such as extension, bending, and twisting, which enables the achievement of special-purpose, high-performance structural requirements. Because these structures are thin walled and are often subjected to compression loads, knowledge of their prebuckling and buckling behaviors is of fundamental importance. A necessary part of fulfilling this need is the development of high-fidelity analysis capabilities and the corresponding validation procedures.

Significant advances in high-fidelity nonlinear finite-element analysis methods and validation-experiment requirements for buckling of thin-walled, laminated-composite cylindrical shells have been made in recent years (e.g., see Ref. 1). These analysis methods are directly applicable to compression-loaded curved panels, but the validation of these high-fidelity analysis methods for curved panels is much less mature. The primary reasons for this lack of maturity, compared to that for compression-loaded cylindrical shells, are that testing of curved panels requires more complex fixtures to facilitate load introduction and edge support, and curved panels require mechanical support of two additional edges. Furthermore, the effects of the test fixture on the load introduction and

[*] Aerospace Engineer, Member AIAA.
[†] Senior Research Engineer, Associate Fellow AIAA.
[‡] Aerospace Engineer, Vehicle Technology Directorate – Army Research Laboratory, Member AIAA.
[§] Aerospace Engineer, Vehicle Technology Directorate – Army Research Laboratory, Member AIAA.

edge support conditions can be difficult to characterize. These issues are significant because the mechanical implementation and characterization of load introduction and edge support conditions used for validation tests can dramatically affect relevancy and usefulness of a validation experiment in the development of practical structural design data. In particular, the test results may not be relevant if the test configuration does not accurately represent the structural configuration in question. Similarly, the test data may be of limited use for model validation purposes if the load introduction and edge support conditions are not accurately characterized and thus are not properly accounted for in the analysis.

Many theoretical and experimental studies that are relevant to validation of high-fidelity analysis methods for bucking of compression-loaded curved panels have been conducted during the last thirty years.[2-8] In particular, these studies have examined the effects of panel curvature, initial geometric imperfections, boundary conditions, and laminate stacking sequence on the buckling behavior. Many of these studies have identified significant discrepancies between the experimentally determined buckling loads and the corresponding analytical buckling predictions. These discrepancies have been attributed to various effects such as improper simulation of boundary conditions, initial geometric imperfections, and initial prestress caused by mismatches between panel and test-fixture geometries. For example, experimental results obtained by Hui[4] for buckling of symmetric cross-ply laminates show that compression-loaded curved panels can exhibit buckling loads greater than the corresponding classical, linear-bifurcation buckling load if an initial geometric imperfection in the form of an outward bulge is present in the panel. This result is in complete agreement, of course, with the unstable, asymmetric bifurcation behavior predicted by even simple analytical methods for compression-loaded curved panels.[9]

Khot and Bauld[5] conducted an experimental study of the buckling response of compression-loaded curved panels made from specially orthotropic laminates that is particularly relevant to the development of validation experiments. In this study, the experimentally measured buckling loads were found to be bounded by the corresponding predicted buckling loads for the case where the circumferential displacements on the curved loaded edges are unrestrained (free circumferential expansion) and for the case where these displacements are fully restrained. The bounding of the experimental buckling loads by the analytical predictions for these two extreme, idealized boundary conditions is attributed to the presence of circumferential slippage of the panel edges in the test fixture, which was observed during the tests. It was also noted in this study that some of the geometrically imperfect panel specimens had to be forced slightly into the more geometrically precise test fixture, which produced initial stress and deformation states prior to compression loading. It was speculated that perhaps these test-fixture-induced states could have an influence on the buckling resistance that is comparable to that of an initial geometric imperfection.

Wilkens[6] conducted extensive buckling tests of compression-loaded, laminated-composite curved panels and indicated that friction between the test fixture and the specimen can affect the panel response. Wilkins minimized the friction that develops between the test fixture and the specimen by bordering the specimen edges with 0.003-in-thick Teflon tape. In addition, Wilkins showed that test-fixture edge supports that are intended to simulate simply supported boundary conditions on the unloaded edges actually provide a slight rotational constraint. For the curved panels he considered, the maximum value of the restraining moment was found to be approximately 10 in.-lb/in. along the length of the panel edge. However, this restraining moment was determined to have a negligible effect on the magnitude of the buckling load of the panels considered.

A recent numerical and experimental study by Hilburger et. al[8] also investigated the effects of friction-induced circumferential edge restraint on the prebuckling and buckling response of compression-loaded, quasi-isotropic curved panels. Specifically, experimental results were obtained that indicated a significant amount of nonlinear prebuckling deformation and experimental buckling loads that are nearly twice the classical linear-bifurcation buckling load predicted by using a finite-element analysis. In addition, the experimental buckling load was found not to be bounded by the corresponding predicted buckling loads for the case where the circumferential displacements on the curved loaded edges are unrestrained (free circumferential expansion) and for the case where these displacements are fully restrained. This inability to bound the results for these two extreme boundary conditions led to the development and use of a finite-element model that simulates test-fixture-induced frictional forces by using circumferentially aligned elastic springs distributed along the curved, loaded edges of the panel. The numerical results obtained with this enhanced finite-element model indicate that a panel with circumferential edge restraint provided by the elastic springs can exhibit significant nonlinear prebuckling deformations that are caused by a nonlinear coupling between the circumferential and out-of-plane displacements near the loaded edges. Additionally, the nonlinear prebuckling deformations result in a net outward bulge of the panel prior to buckling that increases the buckling resistance in the same manner as reported by Hui[4] for initial geometric imperfections.

Moreover, the results obtained by using the springs at the loaded edges appear to more accurately represent the experimentally measured results and suggest that some amount of circumferential restraint of the loaded edges was present in the experimental setup.

The results presented in the literature reviewed herein indicate several factors that must be well understood in order to develop experiments that are adequate for validating analysis methods for laminated-composite curved panels. Three of these factors are the effects of circumferential edge restraint, the effects of rotational edge restraint, and the effects of a mismatch between the panel and test-fixture geometries at the support locations. To a large extant, these effects are not well understood. Thus, the objective of the present study is to quantify these three effects, and their interactions, for the baseline case of a compression-loaded, quasi-isotropic composite curved panel by using high-fidelity nonlinear finite-element analyses. Toward this goal, results of a parametric study are presented that encompass a wide range of circumferential and rotational edge-restraint conditions and initial stress and deformation states associated with forcing a geometrically imperfect panel specimen into a more geometrically precise test fixture, prior to application of the destabilizing compression load. First, the finite-element model and analysis method are described. Then, results that illustrate the individual contributions of each of the three effects on the prebuckling and buckling response are presented and discussed. Lastly, results that show the nonlinear interaction of the three effects are presented.

Finite-Element Model and Analysis Method

The panels considered in this study were analyzed with the STAGS (STructural Analysis of General Shells) nonlinear shell analysis code.[10] STAGS is a finite-element code designed for the static and dynamic analysis of general shells, and includes the effects of geometric nonlinearities in the analysis. A typical finite-element model is shown in Fig. 1. Points making up the panel mid-surface are located by an x-y-z curvilinear coordinate system, with the origin at the center of the panel. The mid-surface axial, circumferential, and out-of-plane displacements are defined as $u(x, y)$, $v(x, y)$, and $w(x, y)$, respectively, as shown in Fig. 1. Here, the term "out-of-plane" refers to the displacement that is normal to the tangent plane at a given point of panel mid-surface. The nominal panel radius R is 60 in. and the panel length L and arc width W are 14.75 in. and 14.5 in., respectively. The panel is modeled as a 24-ply-thick $[\pm 45/0/90]_{3s}$ quasi-isotropic graphite-epoxy laminate with a nominal ply thickness of 0.0054 in. and a total, nominal panel thickness of 0.13 in. The nominal lamina material properties are as follows: longitudinal modulus E_1 = 18.5 Msi, transverse modulus E_2 = 1.62 Msi, inplane shear modulus G_{12} = 0.87 Msi, and major Poisson's ratio ν_{12} = 0.305. Idealizations of the test-fixture support conditions were used in the finite-element model, referred to herein as the nominal boundary conditions, and are defined as follows. On the clamped loaded edges, the out-of-plane displacement w, is set equal to zero in the boundary regions of the finite-element model that extend 3/8 in. from both loaded ends of a panel (see Fig. 1). The compression load is introduced into the panel by applying a uniform end shortening displacement Δ to one end of the model while holding the other end of the panel fixed on the boundary; that is, $u(-L/2, y) = \Delta$ and $u(L/2, y) = 0$. The simply supported boundaries on the unloaded edges (knife-edge supports) were simulated by setting the out-of-plane displacement, w, equal to zero on a line 3/16 in. from each unloaded edge of a panel. The finite-element model uses four-noded, flat facet-type elements that are based on the kinematic hypothesis of Kirchoff-Love thin-shell theory and the nonlinear Lagrangian strain tensor. The element nodes include three translational degrees of freedom (u, v, w) and three rotational degrees of freedom. The rotational degrees of freedom are denoted by r_x, r_y, and r_z and correspond to rotations about the x, y, and z axes, respectively. Large rotations are accounted for by using a co-rotational algorithm.

The STAGS finite-element code uses both the modified and full Newton methods for its nonlinear solution algorithms. The Riks pseudo arc-length path-following method is used to continue a solution past the limit points of a nonlinear response. In this computational approach, the incrementally applied loading parameter is replaced by an arc length along the solution path, which is then used as the independent loading parameter. The arc-length increments are automatically adjusted by the program as a function of the solution behavior.

As mentioned previously, idealized, geometrically perfect panels with nominal boundary conditions and the corresponding panels with elastic boundary restraints and with initial stress and deformation states caused by a mismatch between the panel and test-fixture geometry are considered in the present paper. In particular, two distinct elastic boundary restraints are considered; that is, elastic circumferential and elastic rotational edge restraints. An

elastic circumferential edge restraint was applied to the curved, loaded edge as a "first-order" approximation of the frictional forces generated between the test fixture and the panel specimen. The elastic circumferential edge restraint is simulated in the finite element model by adding a linear spring-stiffness contribution K_v directly to the stiffness of the elements in the curved, loaded boundary that are indicated in Fig. 1. The magnitude of K_v varied from a value of 0.0 lb/in., corresponding to unrestrained circumferential motion, to a relatively high value of 1.0×10^9 lb/in. In addition, complete circumferential restraint at the loaded edges, given by $v = 0$, was also considered. As a point of reference, the circumferential membrane stiffness of the panel is given by $A_{22} = 9.22 \times 10^5$ lb/in.

To better understand the effects of the restraint generated by the knife-edge supports on the unloaded edges of the panels, an elastic rotational edge restraint was applied to each unloaded edge that is representative of a "first-order" approximation to the true support condition. The elastic rotational edge restraint is simulated in the finite-element model by a beam on both sides of the panel that has a prescribed torsional stiffness and values for the bending and extensional stiffness that are equal to zero. The magnitude of the torsional stiffness K_θ varied from a value of 0.0 lb-in, corresponding to completely unrestrained rotation, to a relatively high value of 1.0×10^9 in.-lb In addition, complete rotational restraint at the unloaded edges (i.e., clamped), given by $r_x = 0$, was also considered. As a point of reference, the corresponding circumferential bending stiffness of the panel is given by $D_{22} = 1.2 \times 10^3$ in.-lb

Initial stress and deformation states caused by a mismatch between the panel geometry and the test fixture geometry at the edge supports were also captured in the finite-element models. For conciseness, these states are referred to herein collectively as a prestress state or a prestress condition. For example, the test fixture used in Ref. 8, and modeled in the present study, is made for a 60-in-radius curved panel, however, because of residual stresses from the curing process, the curved laminated-composite test specimens had a measured average constant radius of about 53 to 54 in. Thus, when a panel was inserted into the 60-in-radius fixture, the panel was forced to conform to the shape of the fixture, which generates unknown stresses and deformations in the panel. This misfit condition is modeled by first modeling a stress-free panel with an initial radius of R_i that represents the as-built average panel radius. Then, displacements are applied to the edges of the panel that simulate insertion of the panel into the 60-in-radius test fixture. The deformation associated with inserting the panel in the fixture is accomplished by applying an out-of-plane displacement to all the nodes on the edges that are based on the difference between the initial, as-built panel radius and the test-fixture radius. After the initial stress and deformation states are applied to the panel, the destabilizing compression load is applied by prescribing a uniform end shortening that is increased monotonically from a value of zero.

Model convergence studies and model verification studies were conducted at various stages in the development of the finite-element models to verify the adequacy of each model. Specifically, convergence studies on the mesh refinement were conducted for each panel configuration; e.g., panel configurations with elastic edge restraint only, initial prestress only, and combinations of elastic edge restraint and initial prestress. The convergence criteria used in the study required that the buckling load could not change by more than one percent with additional mesh refinement. In addition, the convergence criteria required that the overall predicted global response characteristics could not change with additional mesh refinement, e.g., the load-shortening response curves and the prebuckling and buckling displacements. The rationale for using a convergence criteria with requirements on the buckling load as well as other global response characteristics is to assure convergence on the correct overall panel response and not just the value for the buckling load. Model verification studies were also conducted to insure that the model inputs were correct. For example, the displacements applied to the clamped boundary region of the panel that were used to simulate the mismatch between the panel and the fixture geometry were verified by comparing the displacements reported in the finite-element model output file with the actual displacement values provided to the analysis code.

Results and Discussion

Numerical results are presented in this section for 60-in-radius, quasi-isotropic panels that are subjected to uniaxial compression loads. First, results are presented that show the effects of elastic circumferential edge restraints that are applied to the curved, loaded edges of the panels. Similar results that have been presented in Ref. 8 by two of the authors are included herein for completeness. Then, results are presented that show the effects of elastic rotational restraints that are applied to the straight, unloaded edges of the panels. Next, results are presented

that show the effects of the initial prestress condition that is caused by the panel-test-fixture misfit. Finally, results are presented that show the interaction effects for various combinations of elastic edge restraint and initial misfit prestress. The values of the axial load P and buckling loads P_{cr} are normalized by the linear-bifurcation buckling load of a geometrically perfect, quasi-isotropic panel with nominal dimensions and boundary conditions and that was obtained from a finite-element analysis; that is, P_{cr}^{o} = 15.78 kips (1 kip = 1000 lbs). Various displacement quantities presented herein are normalized by either the nominal panel thickness, t = 0.13 in., the nominal panel length, L = 14.75 in., or the nominal panel width, W = 14.5 in.

Elastic Circumferential Edge Restraint

Results that show the fundamental effects of elastically restraining the circumferential movement of the loaded edges are presented in Figs. 2-5. Specifically, load-shortening response curves for the geometrically perfect, quasi-isotropic panel with nominal dimensions and different degrees of circumferential restraint on the loaded edges are presented in Fig. 2. The corresponding curves for load versus normalized central out-of-plane displacement δ/t are shown in Fig. 3, where $\delta = w(0, 0)$. Positive values of δ/t correspond to movement of the center of the panel outward, away from the center of curvature. Similarly, the corresponding curves for load versus normalized circumferential displacement v_o/W at one corner of the panel is shown in Fig. 4, where $v_o = v(L/2, -W/2)$. Negative values of v_o/W correspond to circumferential Poisson-like expansion that is normally associated with an axially compressed panel. Two curves are shown in each of Figs. 2-4 that correspond to values of the circumferential edge-restraint stiffness K_v = 0 lb/in. (unrestrained) and $K_v = 10^7$ lb/in., which is approximately 10.8 times the circumferential stiffness A_{22}. A third curve is shown in each figure for the case of complete edge restraint, for which v = 0 at the loaded edges. The curves for K_v = 0 lb/in. also include the results for the postbuckling range of loading. The point at which buckling occurs for each case is marked on the curves with filled circles. Contour plots of the corresponding out-of-plane displacement field at the onset of buckling are shown in Figs. 5a-5c for the three edge-restraint cases. The slight skewing that appears in the contour plots is associated with a relatively small degree of flexural anisotropy.

The results in Figs. 2-4 indicate that the degree of circumferential edge restraint on the curved loaded edges of the compression-loaded panel has a significant effect on the response. For the case of unrestrained edges (K_v = 0), the load-shortening response curve shown in Fig. 2 is linear up to the buckling point at P/P_{cr}^{o} = 0.98. Likewise, the corresponding center out-of-plane displacement shown in Fig. 3 is slightly inward prior to buckling, and the loaded edge of the panel undergoes circumferential expansion (Fig. 4), as expected for a circumferentially unrestrained edge. Near the buckling point, and in the postbuckling range of loading, the magnitude of the center out-of-plane displacement grows rapidly to many times the wall thickness of the panel. For the value of $K_v = 10^7$ lb/in., the load-shortening behavior is significantly different. For this case, the load-shortening response curve (Fig. 2) shows a significant amount of nonlinearity prior to buckling and has a relatively high buckling load of P_{cr}/P_{cr}^{o} = 1.95. This nonlinearity in the response curve is caused by coupling of the circumferential and out-of-plane displacements near the loaded edges, which produce an outward bulge in the panel as the loading increases. The coupling of the displacement fields is indicated in Fig. 4 by the initial, slight circumferential expansion followed by circumferential contraction that is caused by local out-of-plane deformation. The outward bulge is evidenced by the corresponding monotonically increasing central out-of-plane displacement shown in Fig. 3 and the displacement contours shown in Fig. 5b. The outward bulge acts to stiffen the panel, by increasing the moment of inertia in the central region, and raises the buckling resistance in the same manner as reported by Hui[4] for panels with a geometric imperfection in the shape of an outward bulge. For the case with fully restrained loaded edges (v = 0), the panel exhibits much less nonlinearity in its load-shortening response curve (Fig. 2), compared to the curve for $K_v = 10^7$ lb/in. In addition, a less pronounced outward bulge (Figs. 3 and 5c) and a lower buckling load given by P_{cr}/P_{cr}^{o} = 1.52 is predicted for the panel with fully restrained loaded edges. Overall, the results in Fig. 2-5 show that prebuckling deformations retard the onset of buckling and result in increases in the buckling load of about 55% and 99%, with respect to the buckling load predicted for the panel with the loaded edges unrestrained, for the circumferential edge-restraint conditions defined by v = 0 and $K_v = 10^7$ lb/in., respectively. Moreover, the results (Fig. 5) show that the prebuckling deformations are very sensitive to changes in the circumferential boundary condition. For example, the out-of-plane prebuckling displacements shown for the case of unrestrained edges (K_v = 0) are characterized by a large, centrally located ellipse-shaped contours and an inward deformation pattern. For a value of $K_v = 10^7$ lb/in., the predicted displacement contours are characterized by a hour-glass-like pattern, with

maximum displacements on the order of 2.6 times the nominal panel wall thickness (Fig. 5b). For $\nu = 0$, the displacement contours are characterized by a centrally located ellipse-shaped outward deformation pattern and the maximum displacement of about 1.5 times the nominal panel thickness (Fig. 5c). It is very important to note that the results predict that the magnitude of the buckling loads and the severity of the nonlinear prebuckling deformations are not bounded by the corresponding results for the extreme boundary conditions defined by $K_v = 0$ (unrestrained) and $\nu = 0$ (completely restrained), which is contrary to intuition.

The predicted effects of elastic circumferential edge restraint on the magnitude of the buckling load are presented in Fig. 6 as a function of the circumferential stiffness parameter K_v. The buckling load values are marked in the figure by filled square symbols and can be placed into three distinct groups that were found to exhibit similar prebuckling behavioral characteristics. The first group of results is for $0 < K_v < 10^{5.2}$ lb/in. Panels with edge-restraint stiffnesses in this group exhibit a linear prebuckling load-shortening response that is similar to that predicted for $K_v = 0$ that is shown in Fig. 2. The normalized buckling load values for this group are all between 0.98 and 1.15. In addition, these panels exhibit prebuckling displacements similar to those shown in Figs. 3-5 for $K_v = 0$. The second group of results are for panels with edge-restraint stiffnesses in the range $10^{5.2}$ lb/in. $< K_v < 10^{7.2}$ lb/in. Panels in this group are predicted to exhibit significant nonlinearity in their prebuckling response; that is, similar to the response characteristics shown in Figs. 2-5 for the panel with $K_v = 10^7$ lb/in. Specifically, the prebuckling load-shortening response curves exhibit a significant amount of nonlinearity above a load level of $P/P_{cr}^{o} = 0.95$, and the buckling loads are on the order of two times the linear-bifurcation buckling load for the corresponding unrestrained panel. The third group of results are for panels with edge-restraint stiffnesses in the range $K_v > 10^{7.2}$ lb/in. The panels associated with this group are predicted to exhibit response characteristics similar to those predicted for the fully restrained case ($\nu = 0$), as shown in Figs. 2-5. The portion of the curve shown in Fig. 6 for this group converges from above to the value of $P_{cr}/P_{cr}^{o} = 1.52$, which is the value for the fully restrained panel.

Elastic Rotational Edge Restraints

Results that illustrate the effects of elastic rotational edge restraints on the buckling response of a compression-loaded curved panel are presented in Figs. 7-10. Specifically, load-shortening response curves for a compression-loaded panel with different degrees of rotational edge restraint on the straight, unloaded edges of the panel are presented in Fig. 7. The corresponding curves for load versus normalized central out-of-plane displacement δ/t are shown in Fig. 8, where $\delta = w(0, 0)$. Three curves are shown in each of Figs. 7 and 8 that correspond to rotational edge restraint stiffnesses of $K_\theta = 0$ (equivalent to the classical simply supported boundary condition), $K_\theta = 10^3$ in.-lb, and the fully restrained case; that is, $r_x(x, -W/2 + 3/16 \text{ in.}) = r_x(x, W/2 - 3/16 \text{ in.}) = 0$. The buckling points are marked with the filled circles.

The results in Figs. 7 and 8 indicate that the rotational edge restraint has a relatively small effect on the response and the buckling load of the panel. In particular, the load-shortening response curves are linear up to buckling and the buckling loads range from $P/P_{cr}^{o} = 0.98$ to 1.08. The effective postbuckling stiffness increases slightly as the rotational constraint stiffness increases. This increase in postbuckling stiffness is caused by a reduction in the out-of-plane postbuckling deformations in the panel at a given load level, as shown in Fig. 8, and a subsequent increase in the effective load-carrying cross-section of the panel. The results in Fig. 8 indicate that the prebuckling center displacement of the panel is small and inward. However, near the buckling point, and in the postbuckling range of the loading, the center displacement grows rapidly to many times the wall thickness of the panel. For all cases, the predicted out-of-plane displacement contours at the onset of buckling are similar in character to that exhibited by a panel with nominal boundary conditions ($K_v = 0$) and are characterized by a large ellipse-shaped inward deformation pattern (e.g., see Fig. 5a).

A summary of the predicted effects of the rotational edge restraint on the buckling load of the panel is presented in Fig. 9. These results indicate that the buckling load increases very slightly from $P_{cr}/P_{cr}^{o} = 0.98$ to 1.08, as K_θ increases from 0 to 10^9 in.-lb, which is somewhat counterintuitive. This slight increase in the buckling load occurs in a transition zone for 10^2 in.-lb $< K_\theta < 10^4$ in.-lb, in which the panel displacement response near the restrained edge transitions from the response for a simply supported edge to that for a clamped edge. More specifically, displacement traces for the panel with various rotational edge restraints are shown in Fig. 10 and illustrate the effects of the rotational restraint on the deformation response near the unloaded edge of the panel.

These displacement traces are taken at the panel mid-length and span the panel arc from $y = 0$ to $y = W/2$. It is important to point out that the curves shown in this figure are not bounded by the curves that correspond to the classical simply supported and clamped boundary conditions because the curves correspond to different load levels incipient to buckling.

For values of $K_\theta < 10^2$ in.-lb, the displacement response near the rotational restraint is similar to a free-rotation response that occurs with a classical simply supported boundary condition, as indicated in Fig. 10. For 10^2 in.-lb $< K_\theta < 10^4$ in.-lb, the panel exhibits a significant reduction in the rotation near the unloaded edge and a reduction in the magnitude of the out-of-plane deformations at buckling, as compared to the simply supported boundary condition. For $K_\theta > 10^4$ in.-lb, the panel exhibits a similar displacement response to that of the fully restrained edge condition corresponding to $r_x = 0$.

Given the significant variation in the deformation response near the unloaded edge shown in Fig. 10, one might expect a much larger increase in the buckling load with an increase in the degree of rotational edge restraint. To address this expectation, and to understand better the panel behavior, a numerical parametric study of the effects of the panel (length-to-arc-width) aspect ratio, L/W, on the buckling response was conducted. Predicted buckling loads are plotted as a function of L/W for $K_\theta = 0$ and $r_x = 0$ in Fig. 11. The curves shown in this figure are festoon curves, similar to the well-known corresponding festoon curves for buckling of flat, compression-loaded rectangular plates (e.g., see Ref. 11). The results indicate that the sensitivity of the panel response to variations in the degree of rotational restraint is clearly dependent on the panel aspect ratio. In addition, the results show that the particular panel configuration considered herein exhibits a relatively small difference between the buckling load for a panel with clamped unloaded edges and the buckling load of a panel with simply supported unloaded edges, at $L/W = 1.02$. Comparing these curves with the corresponding curves shown in Ref. 11 for flat isotropic plates suggests that panel curvature amplifies the effect of clamping the loaded edges of the panels to the extent that the differences in buckling load associated with restraining the unloaded edges becomes much less significant. This behavior would account for the relatively benign variation in buckling load with K_θ that is shown in Fig. 9.

Initial Misfit Prestress

Results that illustrate the effects of an initial misfit prestress (also referred to herein as an initial panel misfit) on the buckling response of the compression-loaded, quasi-isotropic curved panels considered herein are presented in Figs. 12-17. As discussed previously, the initial misfit prestress is caused by a mismatch between a 60-in-radius test fixture and a stress-free panel with a different initial radius R_i, and is comprised of panel deformations and stresses that result from forcing the panel to conform to the 60-in-radius fixture. Displacement contours associated with the initial prestress of panels with initial radii R_i equal to 52-in., 56-in., and 64-in. are presented in Fig. 12. Each panel configuration has two displacement contour plots associated with it. The first contour plot for each panel (Figs. 12a-1, 12b-1, and 12c-1) shows the actual deformation response that results from placement in the test fixture, as measured with respect to corresponding initial, undeformed geometry. The second contour plot for each panel (Figs. 12a-2, 12b-2, and 12c-2) shows the deformed panel geometry, as measured with respect to a geometrically perfect 60-in-radius panel and is analogous to an initial geometric imperfection shape that is commonly used in shell buckling analyses. In general, the results indicate that the initial prestress deformations of the panels with $R_i < 60$ in. are outward bulges with magnitudes equal to 1-3% of the nominal wall thickness (see Figs. 12a-2, 12b-2). In contrast, panels with $R_i > 60$ in. exhibit initial prestress deformations that are inward bulges, as shown in Fig. 12c-2. In addition, initial inplane stress resultants and moment resultants were predicted for each case (not presented herein) and indicate that the stresses caused by forcing the panels into the test fixture are typically several orders of magnitude smaller than the corresponding stresses at the onset of buckling.

Load-shortening response curves for panels with different amounts of prestress are presented in Fig. 13. The corresponding curves for load versus normalized central out-of-plane displacement δ/t are shown in Fig. 14, where $\delta = w(0, 0)$. Similarly, the corresponding curves for load versus normalized circumferential displacement v_o/W at one corner of the panel are shown in Fig. 15, where $v_o = v(L/2, -W/2)$. The initial center displacements and circumferential displacements for $P/P_{cr}^o = 0$ in Figs. 14 and 15 are attributed to the initial prestress deformation response that occurs in the panels before the compression load is applied. Four curves are shown in each of Figs.

13-15 that correspond to panels with initial radii R_i equal to 52 in., 56 in., 60 in. (no prestress), and 64 in., and illustrate the overall effects of an initial prestress on the compression response. The buckling points are marked with filled circles.

The results in Figs. 13-15 indicate that the level of initial prestress in the panel has a significant effect on the prebuckling response. Panels with R_i = 60 in. (no prestress) and 64 in. exhibit linear prebuckling load-shortening response curves and have normalized buckling loads of 0.98, and 0.90, respectively. Likewise, the corresponding center out-of-plane displacement shown in Fig. 14 is small and inward prior to buckling, with the displacements for the 60-in. panel being practically negligible, and the load edges undergo circumferential expansion, as shown in Fig. 15. The panel with R_i = 56 in. exhibits a similar linear prebuckling load-shortening response and has normalized buckling loads of 1.17. However, the corresponding center out-of-plane displacement shown in Fig. 14 is small and outward prior to buckling. In addition, the load edge initially undergoes circumferential expansion followed by slight circumferential contraction at approximately P/P_{cr}^{o} = 1.02, as shown in Fig. 15. For a panel with an initial radius R_i = 52 in., the behavior is significantly different. For this case, the panel exhibits a significant increase in the nonlinearity of the prebuckling response beyond a load level of P/P_{cr}^{o} = 1.2 and buckles at P/P_{cr}^{o} = 1.80. This nonlinearity in the response is caused by a coupling between the out-of-plane and circumferential displacements near the loaded edges of the panel, which produces an outward central displacement of the panel as loading increases. The strong coupling of the displacement fields is indicated in Fig. 15 by the initial, slight circumferential expansion followed by circumferential contraction that is caused by local bending. The outward prebuckling deformation is evidenced by the corresponding monotonically increasing central out-of-plane displacement shown in Fig. 14 and the displacement contours shown in Fig. 16a. This response is similar in character to the response previously described for a geometrically perfect panel with a tangential, loaded-edge stiffness given by K_v = 1.0 x 10^7 lb/in.(see Figs 2-5). Overall, the results for R_i = 52 in. and 56 in. shown in Figs. 13-16 indicate that the outward prebuckling deformations retard the onset of buckling and result in increases in the buckling load of about 84% with respect to the buckling load of the panel with no initial prestress. Moreover, the results in Fig. 16 indicate that the prebuckling displacement response can change significantly as the initial prestress in the panel changes. In particular, the results show that panels with $R_i \leq$ 55 in. exhibit prebuckling displacements that are characterized by an hour-glass-like pattern with maximum displacements of approximately three times the nominal panel wall thickness, as shown in Fig. 16a. This displacement pattern is very similar to that exhibited by the corresponding geometrically perfect panel with the circumferential edge restraint $K_v = 10^7$ lb/in. that is shown in Fig. 5b. Panels with 55 in. < R_i < 60 in. exhibit prebuckling deformations that are characterized by a large centrally located ellipse-shaped outward deformation pattern with maximum displacements of approximately 60% of the nominal panel wall thickness, as shown in Fig. 16b. This displacement pattern is very similar to that of the corresponding geometrically perfect panel with the fully restrained circumferential edge condition, v = 0, shown in Fig. 5c. Finally, panels with R_i = 64 in. exhibit a prebuckling displacement response that is characterized by a large centrally located ellipse-shaped inward deformation pattern, as shown in Fig. 16c, that is similar to that of a geometrically perfect panel with a circumferential edge restraint that ranges from $0 < K_v < 10^3$ lb/in., as shown in Fig. 5a.

The predicted effects of the initial, test-fixture induced prestress on the magnitude of the buckling load of the panel are summarized in Fig. 17. The buckling load values are marked in the figure by filled square symbols and can be divided into three groups; that is, R_i < 55 in., 55 in. < R_i < 60 in., and R_i > 60 in. In general, panels with $R_i \geq$ 60 in. exhibit a linear prebuckling load-shortening response and inward prebuckling displacements similar to those predicted for panels with R_i = 60 in. and 64 in. that are shown in Figs. 13-16. The buckling-load values for this group range from P_{cr}/P_{cr}^{o} = 0.88 to 0.98. Panels with 55 in. < R_i < 60 in. exhibit linear prebuckling load-shortening response and outward prebuckling displacements similar to those predicted for panels with R_i = 56 in., as shown in Figs. 13-16. The buckling load values for this group range from P_{cr}/P_{cr}^{o} = 1.1 to 1.2. Finally, panels with R_i < 55 in. exhibit significant nonlinearity in their prebuckling response; that is, similar in character to the response shown in Figs. 13-16 for R_i = 52 inches. In particular, the prebuckling load-shortening response curves exhibit a significant amount of nonlinearity above a load level of P/P_{cr} = 1.2, the prebuckling deformations are outward, and the buckling loads are on the order of two times the linear-bifurcation buckling load for the corresponding geometrically perfect panel with no initial prestress.

Combined Effects of Initial Misfit Prestress and Elastic Edge Restraints

Selected results illustrating the combined effects of an initial misfit prestress and elastic edge restraints on the compression response of a 60-in-radius, quasi-isotropic panel are presented in Figs. 18-21. More specifically, buckling loads for initial panel radii given by R_i = 52 in., 56 in., 60 in., and 64 in. are presented in Figs. 18a, 18b, 18c, and 18d, respectively. Each figure presents normalized buckling loads as a function of rotational restraint stiffness, K_θ, and contains seven curves that correspond to different degrees of circumferential restraint on the loaded edges of the panel. In general, the results indicate that there is a significant amount of nonlinear coupling between the two elastic edge restraint conditions and the test-fixture-induced prestress. The results can be subdivided in to three major groups that correspond to various combinations of parameters K_v, K_θ, and R_i that are affecting the response. Group 1 is associated with panel responses that are affected by variations in K_v only and correspond to panel configurations with $K_\theta > 10^4$ in.-lb and for all values of initial radius considered herein. The effects of K_v on the panel response has already been presented herein and, as a results, will not be discussed in this section, since it was covered in one of the earlier sections. Group 2 is associated with panel responses that are affected by a combination of K_v and initial prestress and corresponds to all panel configurations with $K_\theta < 10^2$ in.-lb. Group 3 is associated with panel responses that are affected by a combination of K_v, K_θ, and initial prestress and include panel configurations with 10^2 in.-lb $< K_\theta < 10^4$ in.-lb. The overall behavioral characteristics associated with the panels in Groups 2 and 3 are described next.

Typical predicted effects of initial prestress and circumferential edge restraint on the buckling loads of panels in Group 2, panels that are affected by a combination of K_v and initial prestress for $K_\theta < 10^2$ in.-lb, are presented in Fig. 19. The results in this figure are for $K_\theta = 0$. In general, the results indicate that the buckling loads of panels with $R_i \geq 56$ in. exhibit a similar dependency on the circumferential edge restraint K_v as geometrically perfect panels with the circumferential edge restraint only (see Figs. 2-5 and the related discussion). However, the prestress can affect the value of the circumferential edge restraint stiffness at which the panels transition from linear prebuckling behavior, associated with the relatively low buckling-load values of 0.98 to 1.15, to nonlinear prebuckling behavior, associated with the relatively high buckling-load values that range from 1.8 to 2.0. For panels with $R_i \leq 54$ in. and $K_v < 10^8$ lb/in., the response is primarily governed by the initial prestress and exhibits characteristics similar to those exhibited by the panels with only an initial prestress (see Figs. 12-17 and the related discussion).

The response of the panels in Group 3 are affected by a combination of edge restraint conditions and initial prestress for values of 10^2 in.-lb $< K_\theta < 10^4$ in.-lb. Within this group there are two subgroups; Group 3-1 for panels with $K_v < 10^5$ lb/in. and Group 3-2 for panels with $K_v > 10^5$ lb/in. The panels in Group 3-1 with R_i = 52 in. exhibit nonlinear prebuckling behavior similar to that shown previously for a panel with $K_v = 10^7$ lb/in (see Figs. 2-5 and the corresponding discussion), and this behavior is characterized by large-magnitude, outward prebuckling deformations and buckling-load levels that approach 1.9 times the classical linear-bifurcation buckling load of the nominal panel, as shown in Fig. 18a. However, as R_i increases, the panel response transitions to one that is characterized by a linear prebuckling response similar to that exhibited by a panel with nominal boundary conditions (see Figs. 2-5 and the corresponding discussion for $K_v = 0$), with relatively small inward prebuckling deformations and normalized buckling load levels between 0.90 and 1.08. Furthermore, the value of K_θ at which this transition from linear to nonlinear prebuckling behavior occurs is a function of the panel prestress and circumferential edge restraint K_v, as indicated in Figs. 18a through 18d. The buckling loads for panels in Group 3-2 (10^2 in.-lb $< K_\theta < 10^4$ in.-lb and $K_v > 10^5$ lb/in.) are influenced strongly by variations in the elastic edge restraints and to a lesser extent by the prestress, as shown Figs. 18a through 18d. In particular, the curves for this class of panels exhibit a festoon-like behavior that is analogous to the curves associated with buckling of flat compression-loaded, finite-length rectangular plates (for example, see Brush and Almroth[11]). This festoon-like behavior is attributed to a distinct change in prebuckling and buckling response characteristics with an increase in the magnitude of the rotational edge restraint. For example, a panel with R_i = 52 in., $K_v = 10^8$ lb/in., and $K_\theta = 10^2$ in.-lb exhibits response characteristics similar to those of a panel with $v = 0$ on the loaded boundaries (e.g., see Figs. 2-5). The response is characterized by a nonlinear prebuckling load-shortening curve, a normalized buckling-load value that ranges from P_{cr}/P_{cr}^o = 1.5 to 1.6, and a large centrally located, ellipse-shaped deformation pattern at the onset of buckling (e.g., see Fig. 20a). As K_θ is increased to $10^{2.7}$ in.-lb, the prebuckling response changes to become more like that of a panel with $K_v = 10^7$

lb/in. (e.g., see Figs. 2-5). This response is characterized by a nonlinear prebuckling load-shortening curve, a normalized buckling-load value that ranges from P_{cr}/P_{cr}^{o} = 1.80 to 1.98, and an hour-glass-shaped deformation pattern at the onset of buckling (e.g., see Fig. 20b). If K_θ is increased further to 10^4 in.-lb, the prebuckling response changes once again. In particular, the buckling load is reduced from around 1.98 to 1.5 and the magnitude of the maximum out-of-plane displacement decreases from 2.4 times to 1.0 times the nominal panel wall thickness, as shown in Fig. 20c. In addition, the character of the initial buckling displacements changes significantly. Specifically, for a panel with $K_\theta = 10^2$ in.-lb, buckling initiates near the loaded edges of the panel, as illustrated by the initial buckling displacement contours shown in Fig. 21a. These displacement contours illustrate, qualitatively, the change in the panel displacements at the onset of buckling and are determined by subtracting the initial buckling displacement field from the displacement field of previous solution step just prior to buckling and, as a result, are referred to herein as Δw contours. Displacement magnitudes are omitted from the plot because the displacement contours are intended to represent an infinitesimal change in the displacements in the neighborhood of the buckling point. For $K_\theta = 10^{2.7}$ in.-lb, the results indicate that buckling initiates near the unloaded boundary of the panel, as indicated by the initial buckling displacement contours shown in Fig. 21b. In contrast, the initial-buckling displacements shown in Fig. 20c for the panel with $K_\theta = 10^4$ in.-lb show that buckling initiates in the center of the panel.

Concluding Remarks

A parametric study of the effects of test-fixture-induced initial prestress and elastic edge restraints on the prebuckling and buckling responses of a compression-loaded quasi-isotropic curved panel has been presented. Highly accurate numerical results were obtained by using a geometrically nonlinear finite-element analysis code and high-fidelity models. Idealizations of the circumferential loaded-edge restraint and the rotational unloaded-edge restraint provided by the test fixture were included in the finite-element models to obtain insight into response-trend variations observed in previously conducted experiments. In addition, the effects of initial stress and deformations states, referred to herein as initial prestress, that result from a mismatch in radius of curvature between a test specimen and the test fixture were simulated analytically.

Several of the effects of the test-fixture-induced initial prestress and elastic edge restraints have been presented, described, and discussed. The results clearly indicate significant effects of the initial prestress and the two types of elastic edge restraint on the panel response in many cases. In particular, the results indicate that the initial prestress and elastic edge restraints can produce significant nonlinear prebuckling deformations in the panel that result in a substantial increase in the buckling resistance of the panel. In addition, the results indicate that various combinations of the initial prestress and elastic edge restraints can exhibit strong coupling and affect the overall nonlinear response of the panel in several different ways. Specifically, the predicted results can generally be categorized into three groups that exhibit distinct behavioral characteristics, depending on the relative degrees of the initial prestress and the elastic edge restraints. For some combinations of initial prestress and edge restraints, the panel exhibits a linear load-shortening response prior to buckling. The prebuckling deformations are negligible and the magnitude of the buckling load for these panels is typically very near the corresponding buckling load obtained from a linear-bifurcation buckling analysis. For other combinations of the initial prestress and edge restraints, the panel exhibits significant nonlinear prebuckling deformations and buckling loads that approach two times the corresponding linear bifurcation buckling load. For still other combinations of initial prestress and edge restraints, the panels exhibit relatively mild prebuckling nonlinearities and typically have buckling loads that are approximately 40% to 60% higher than the corresponding linear-bifurcation buckling load.

Overall, the results indicate, in a quantitative manner, how laminated-composite, curved-panel test specimens that are subjected to compression loads can exhibit significant sensitivity to the degree of circumferential and rotational edge restraint provided by a test fixture and the initial stress and deformation states that result from a relatively slight mismatch in the specimen and test-fixture geometries. Thus, great care must be taken when developing and implementing a test program for this type of structural configuration. Furthermore, since several combinations of initial prestress and edge restraints can result in similar response characteristics and buckling resistance, one must be careful to accurately characterize all pertinent aspects of the test fixture and panel specimen

before each test in order to have adequate information needed to assess the influence of each factor on the panel response.

In addition to the fundamental information presented herein that is relevant to structural testing, the results also provide insight into enhancements in buckling resistance that can be achieved by tailoring the support conditions for curved panels. The results presented herein should also be of particular interest to engineers and designers involved in simulating flight-hardware boundary conditions in structural verification and certification tests, and to scientists and engineers involved in validating structural analysis tools.

References

1. Hilburger, M. W., Starnes, J. H. Jr., "Effects of Imperfections on the Buckling Response of Composite Shells," *Thin-Walled Structures*," Vol. 42, 2004, pp. 369-397.
2. Snell, M. B. and Morley, N. T., "The Compression Buckling Behaviour of Highly Curved Panels of Carbon Fibre Reinforced Plastic," *Proceedings of the Fifth International Conference on Composite Materials*, ICCM Vol. 5, 1985, pp. 1327-1354.
3. Leissa, A. W., "Buckling of Laminated Composite Plates and Shell Panels," *Report AFWAL-TR-85-3069*, AF Wright Aeronautical Laboratories, June 1985.
4. Hui, D., "Asymmetric Postbuckling of Symmetrically Laminated Cross-ply Short Cylindrical Panels Under Compression," *Composite Structures*, Vol. 3, 1985, pp. 81-95.
5. Khot, N. S., and Bauld, N. R., Jr., "A Numerical and Experimental Investigation of the Buckling Behavior of Composite Panels." *Computers and Structures*, Vol. 15, No. 4, 1982, pp. 393-403.
6. Wilkins, D. J., "Compression Buckling Tests of Laminated Graphite-Epoxy Curved Panels," *AIAA Journal*, Vol. 13, No. 4, 1975, pp. 465-470.
7. Knight, N. F. and Starnes, J. H. Jr., "Postbuckling Behavior of Selected Graphite-Epoxy Cylindrical Panel Loaded In Compression," *Proceedings of the AIAA/ASME/ASCE/AHS 27th Structures, Structural Dynamics, and Materials Conference*, AIAA paper 86-0881-CP, 1986.
8. Hilburger, M. W., Britt, V. O., and Nemeth, M. P., "Buckling Behavior of Compression-Loaded Quasi-Isotropic Curved Panels With a Circular Cutout," *International Journal of Solids and Structures*, Vol. 38, 2001, pp.1495-1522.
9. Librescu, L., Nemeth, M. P., Starnes, J. H., Jr., and Lin, W., "Nonlinear Response of Flat and Curved Panels Subjected to Thermomechanical Loads," *Journal of Thermal Stresses*, Vol. 23, 2000, pp. 549-582.
10. Rankin, C. C., Brogan, F. A., Loden, W. A., and Cabiness, H. D., "STAGS Users Manual, Version 4.0," Lockheed Martin Missiles & Space Co., Inc., Advanced Technology Center, Report LMSC P032594, May 2001.
11. Brush, D. O., and Almroth, B., O., *Buckling of Bars, Plates, and Shells*, McGraw Hill, 1975, p. 97.

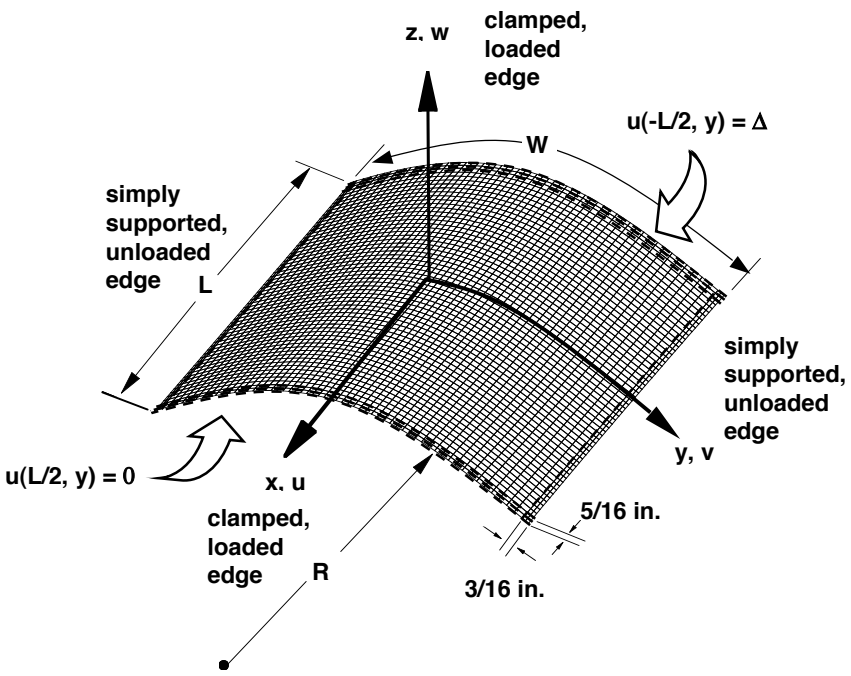

Fig. 1 Typical model geometry and boundary conditions (dashed lines mark the rows and columns where the boundary conditions are applied).

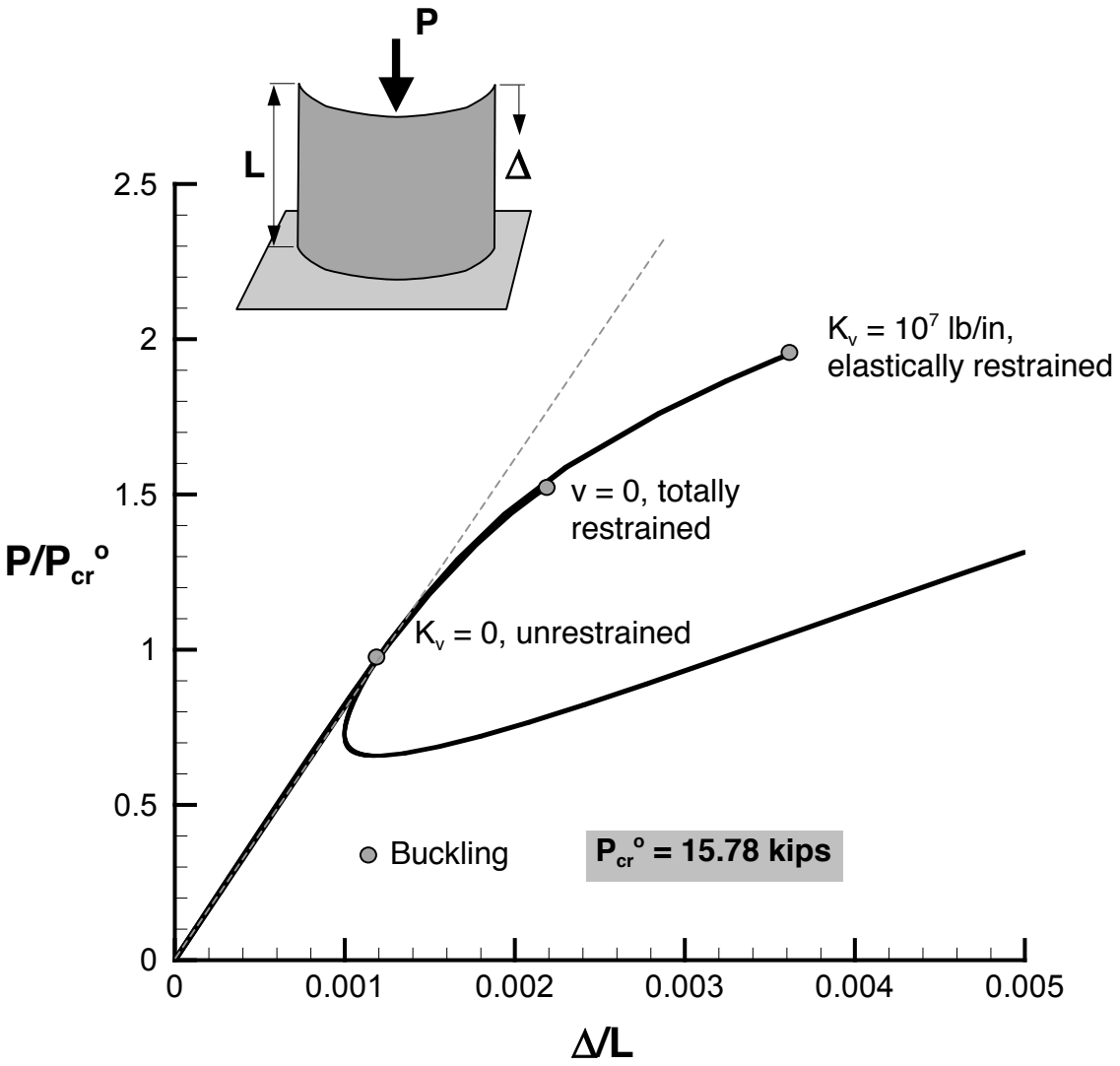

Fig. 2 Effects of circumferential loaded-edge restraint on the load-shortening response of a compression-loaded, 60-in. radius, quasi-isotropic panel.

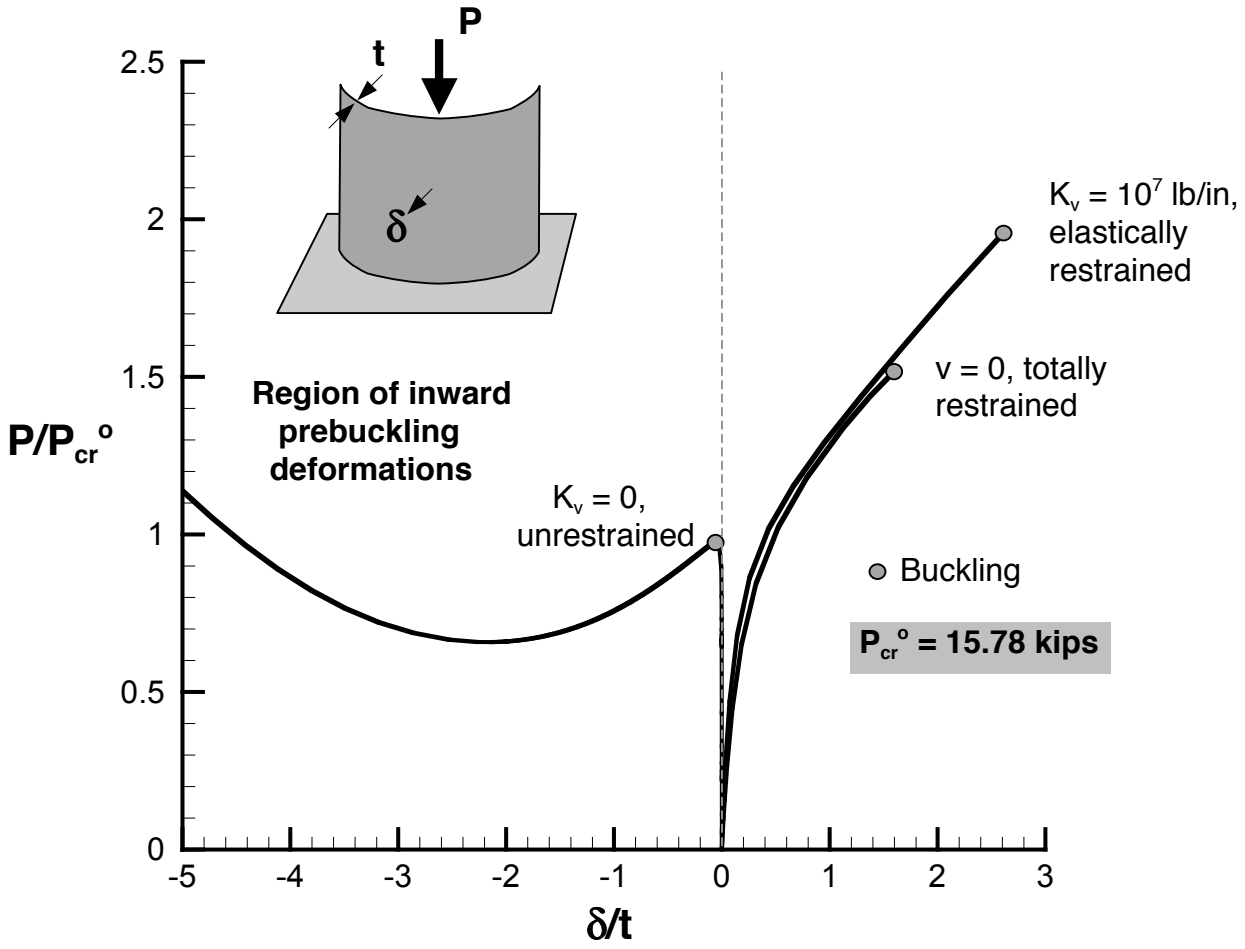

Fig. 3 Effects of circumferential loaded-edge restraints on the out-of-plane center displacement of a compression-loaded, 60-in. radius, quasi-isotropic panel.

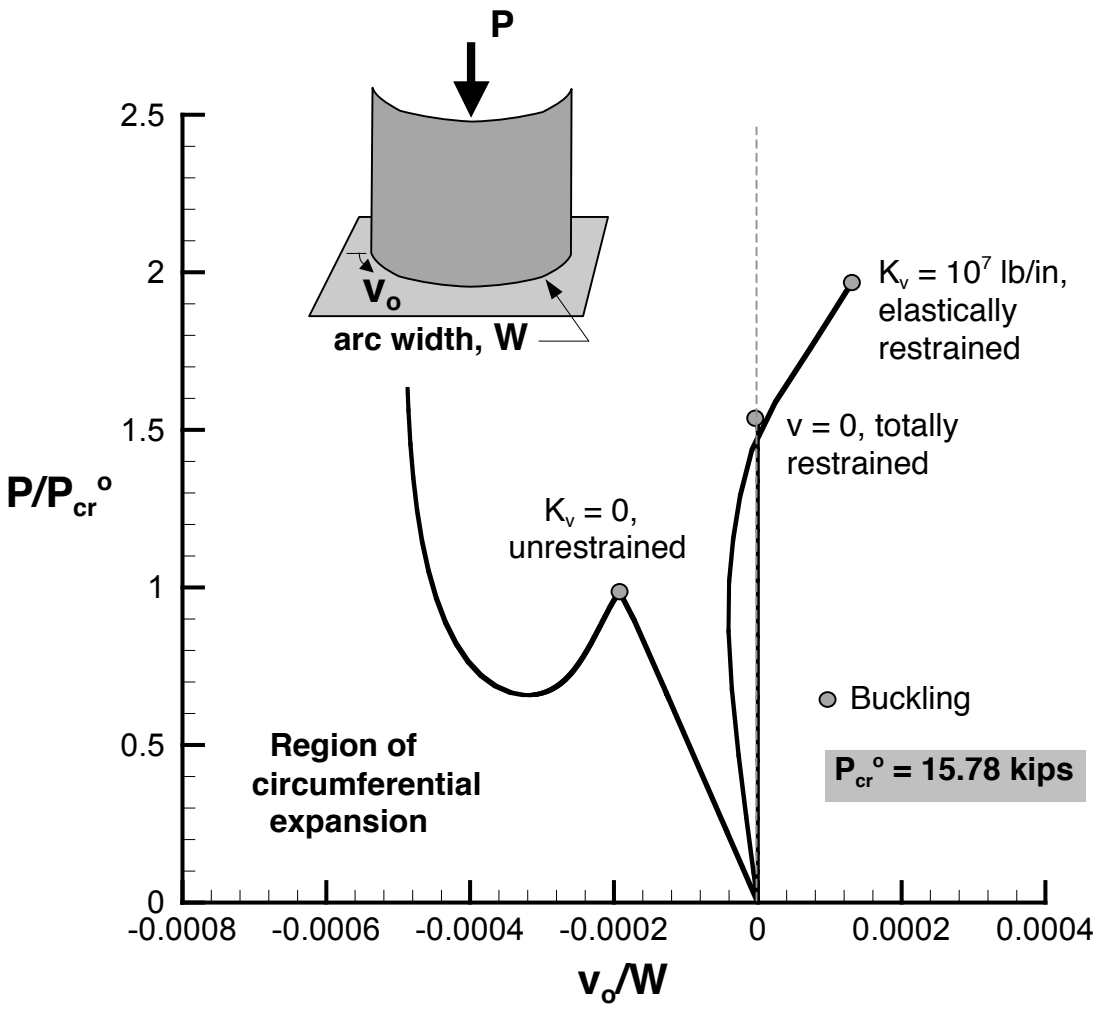

Fig. 4 Effects of circumferential loaded-edge restraint on the circumferential of displacement of a compression-loaded, 60-in. radius, quasi-isotropic panel.

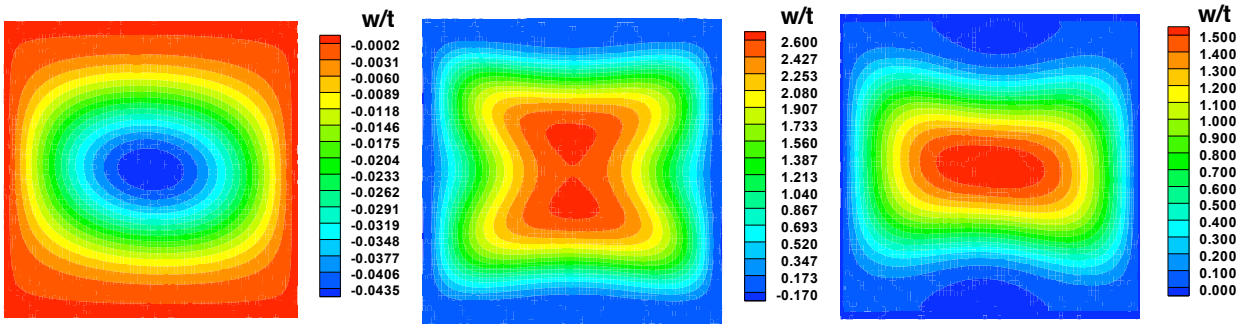

(a) $K_v = 0$, $P/P_{cr}^o = 0.98$ (b) $K_v = 10^7$ lb/in., $P/P_{cr}^o = 1.95$ (c) v = 0, clamped, $P/P_{cr}^o = 1.52$

Fig. 5 Effects of circumferential boundary stiffness K_v on the out-of-plane displacements at the onset of buckling of a 60-in. radius, quasi-isotropic panel (P_{cr}^o = 15.78 kips).

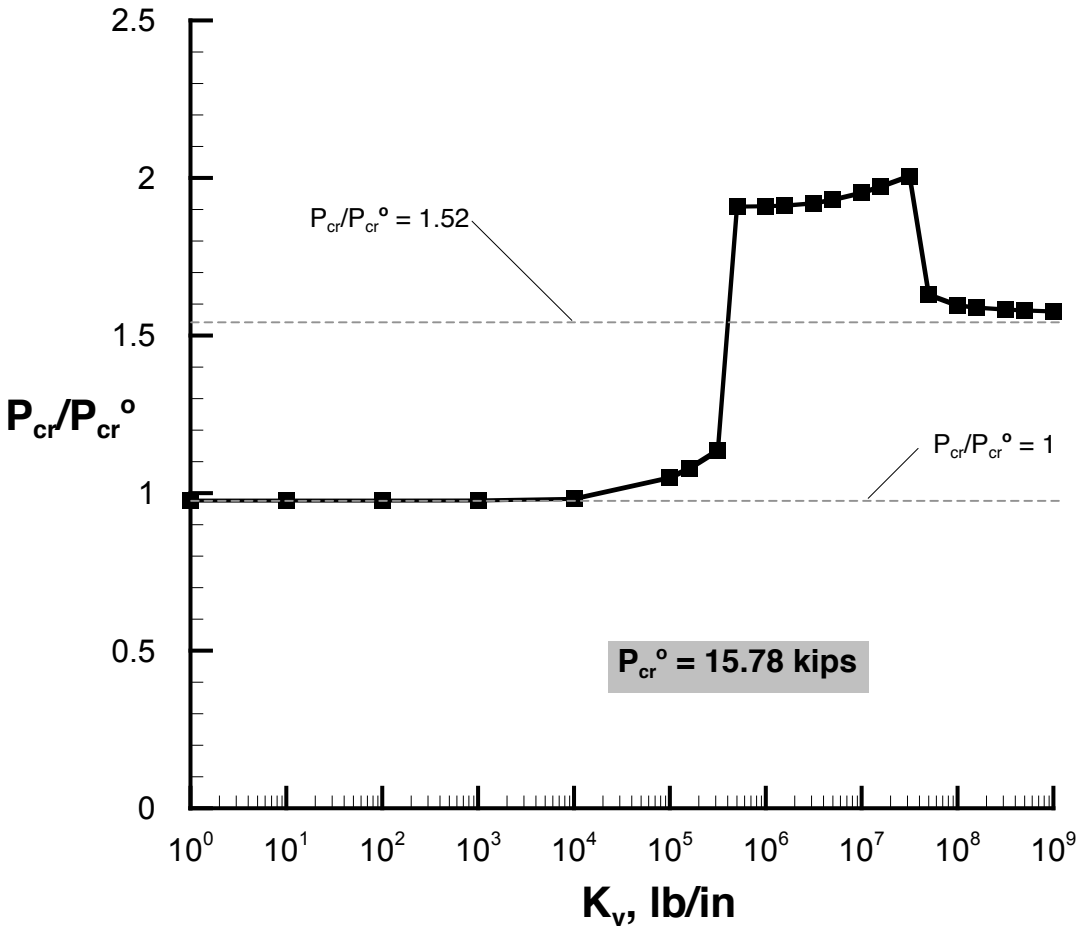

Fig. 6 Effects of circumferential edge restraints on the buckling load of a compression-loaded, 60-in. radius, quasi-isotropic panel.

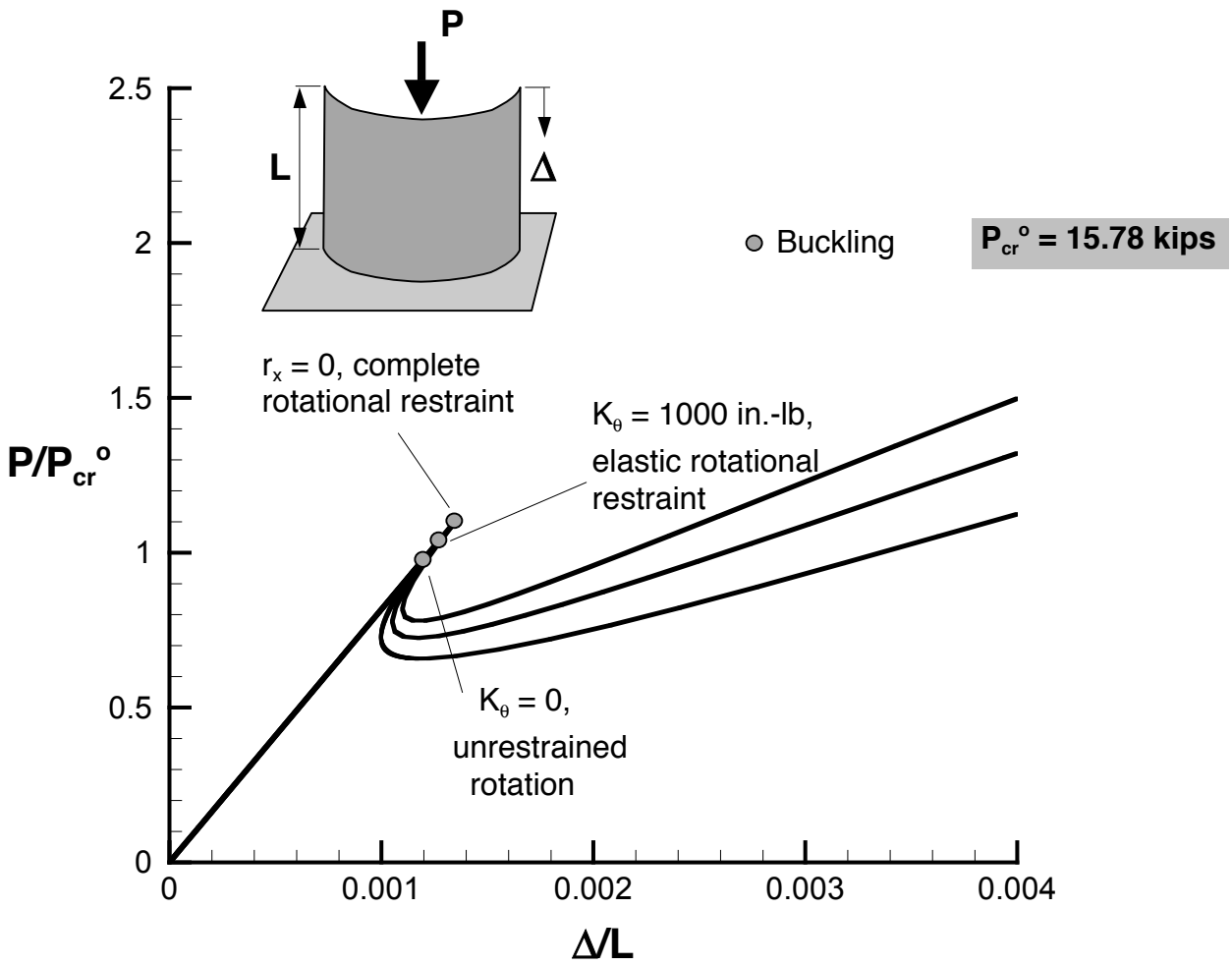

Fig. 7 Effects of rotational unloaded-edge restraint on the load-shortening response of a compression-loaded, 60-in. radius, quasi-isotropic panel.

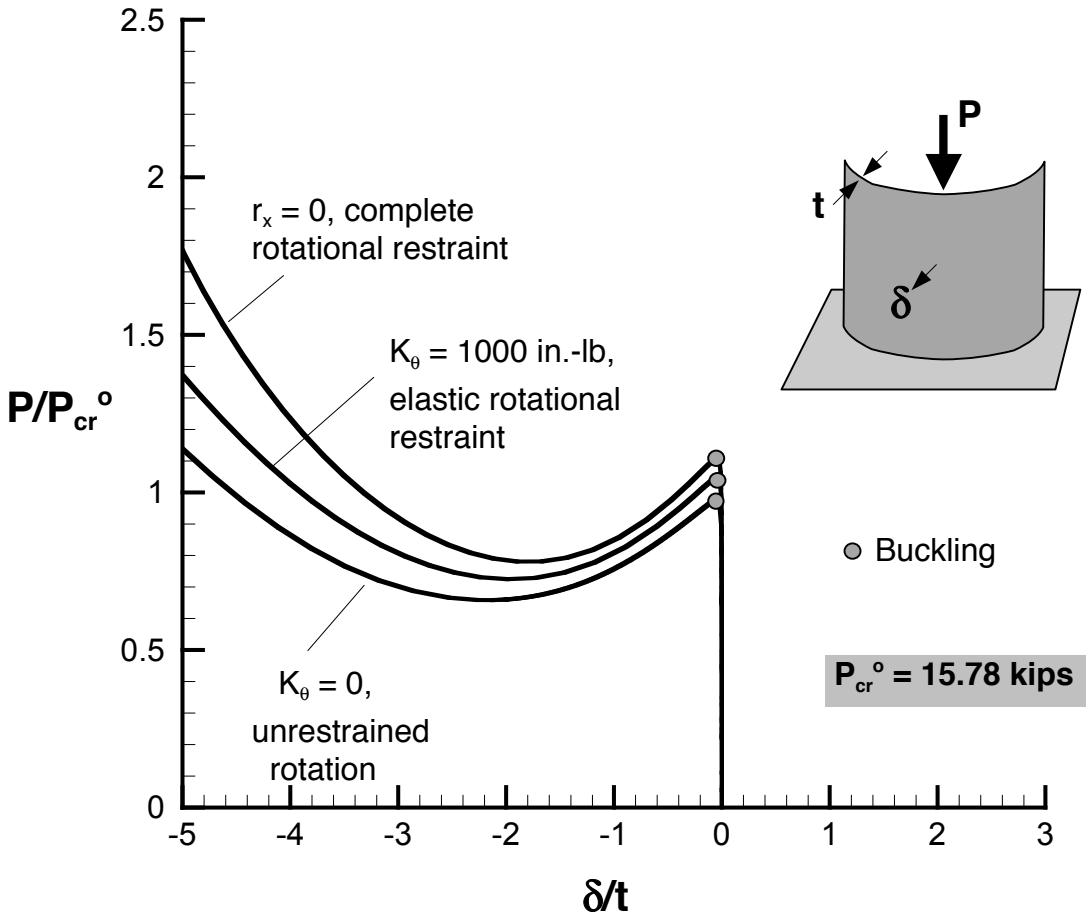

Fig. 8 Effects of rotational unloaded-edge restraint on the out-of-plane center displacement of a compression-loaded, 60-in. radius, quasi-isotropic panel.

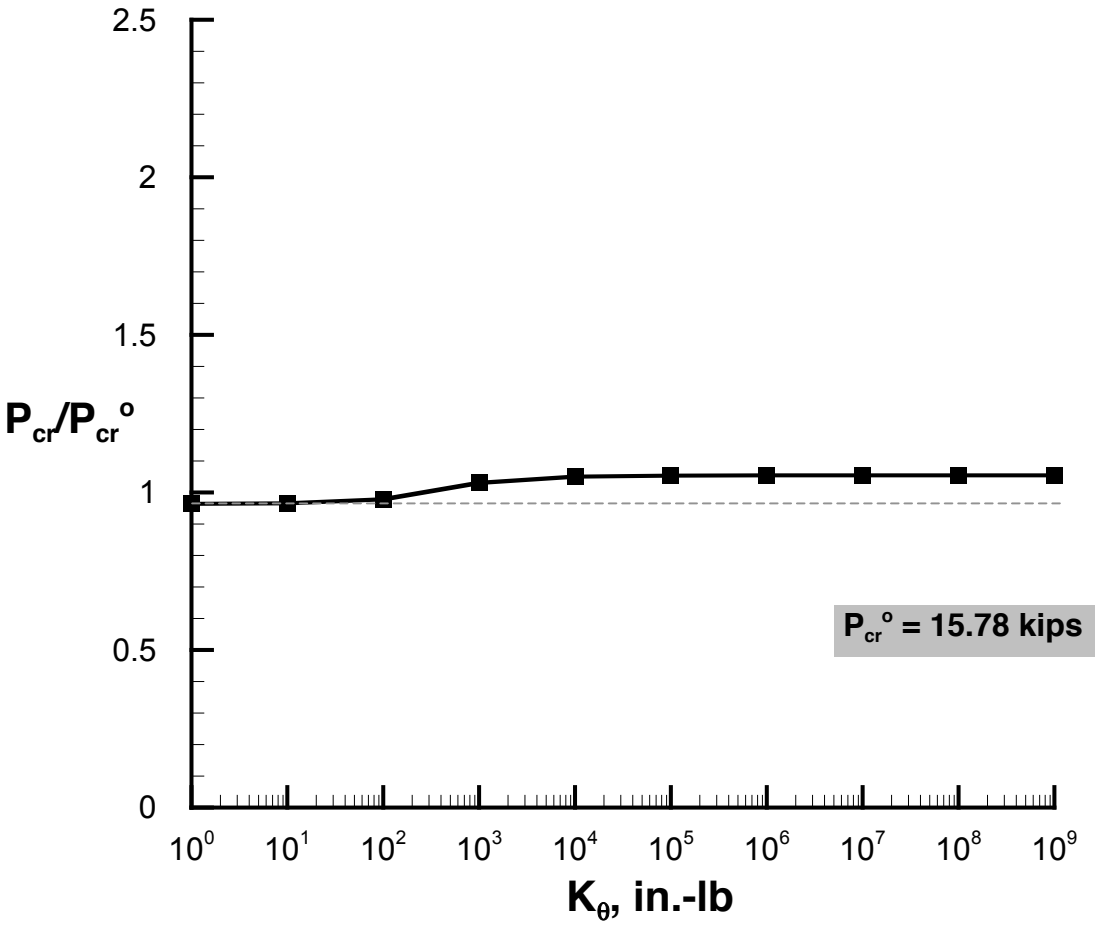

Fig. 9 Effects of rotational unloaded-edge restraint on the buckling load of a compression-loaded, 60-in. radius, quasi-isotropic panel.

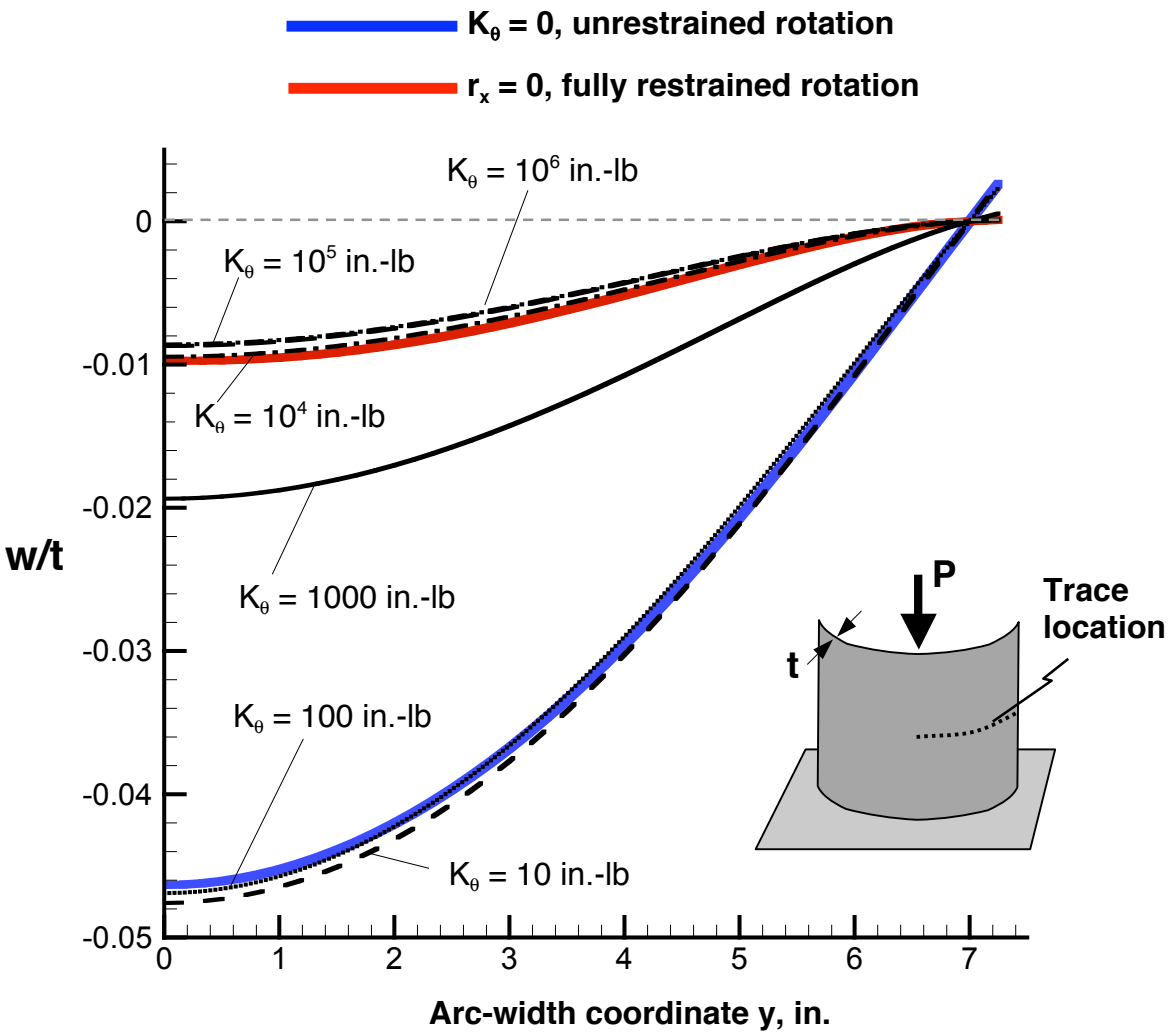

Fig. 10 Effects of the rotational unloaded-edge restraint on the mid-length panel deformations of a compression-loaded, 60-in. radius, quasi-isotropic panel.

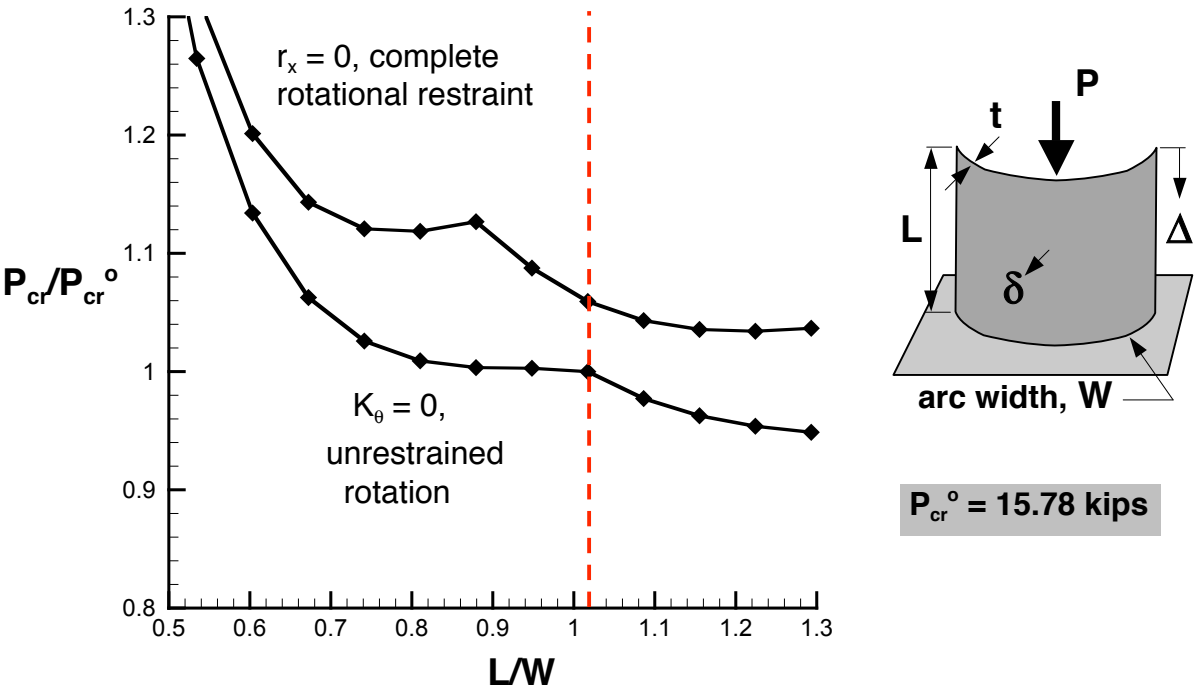

Fig. 11 Effects of panel aspect ratio L/W on the buckling load of panels with simply supported ($K_\theta = 0$) and clamped ($r_x = 0$) boundary conditions on the unloaded edges of a compression-loaded, 60-in. radius, quasi-isotropic panel.

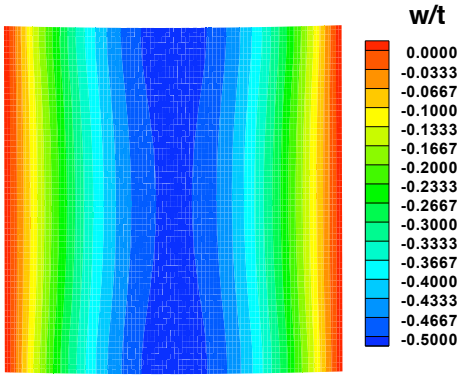

(a-1) R_i = 52 in., referenced to the initial undeformed geometry

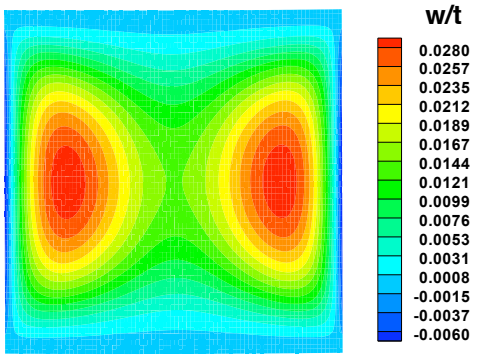

(a-2) R_i = 52 in., referenced to a geometrically perfect 60-in-radius panel

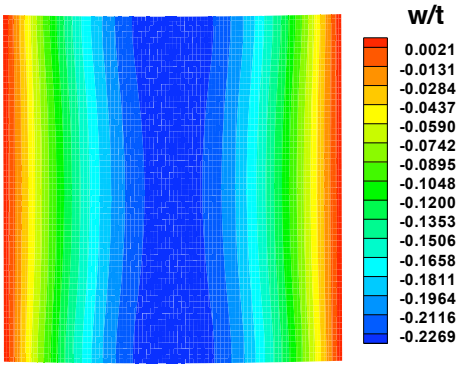

(b-1) R_i = 56 in., referenced to the initial undeformed geometry

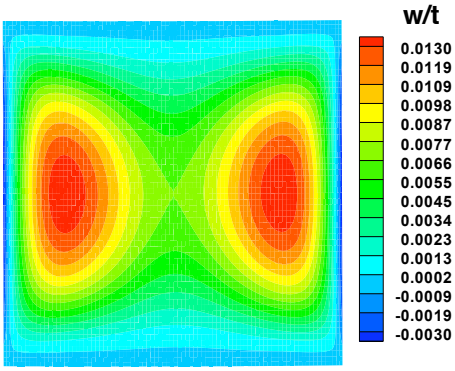

(b-2) R_i = 56 in., referenced to a geometrically perfect 60-in-radius panel

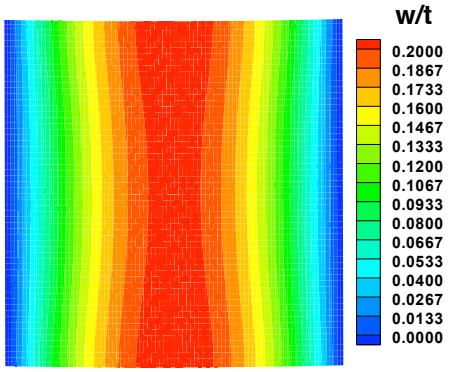

(c-1) R_i = 64 in., referenced to the initial undeformed geometry

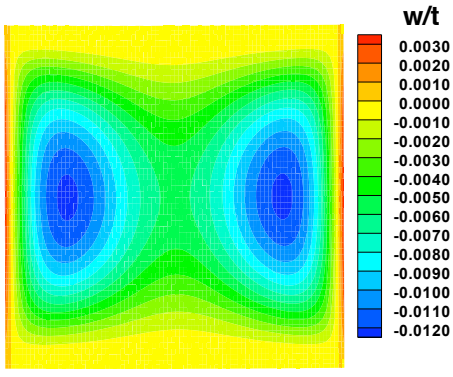

(c-2) R_i = 64 in., referenced to a geometrically perfect 60-in-radius panel

Fig. 12 Effects of initial radius R_i on the prestress displacements of a quasi-isotropic curved panel placed into a 60-in. radius test fixture.

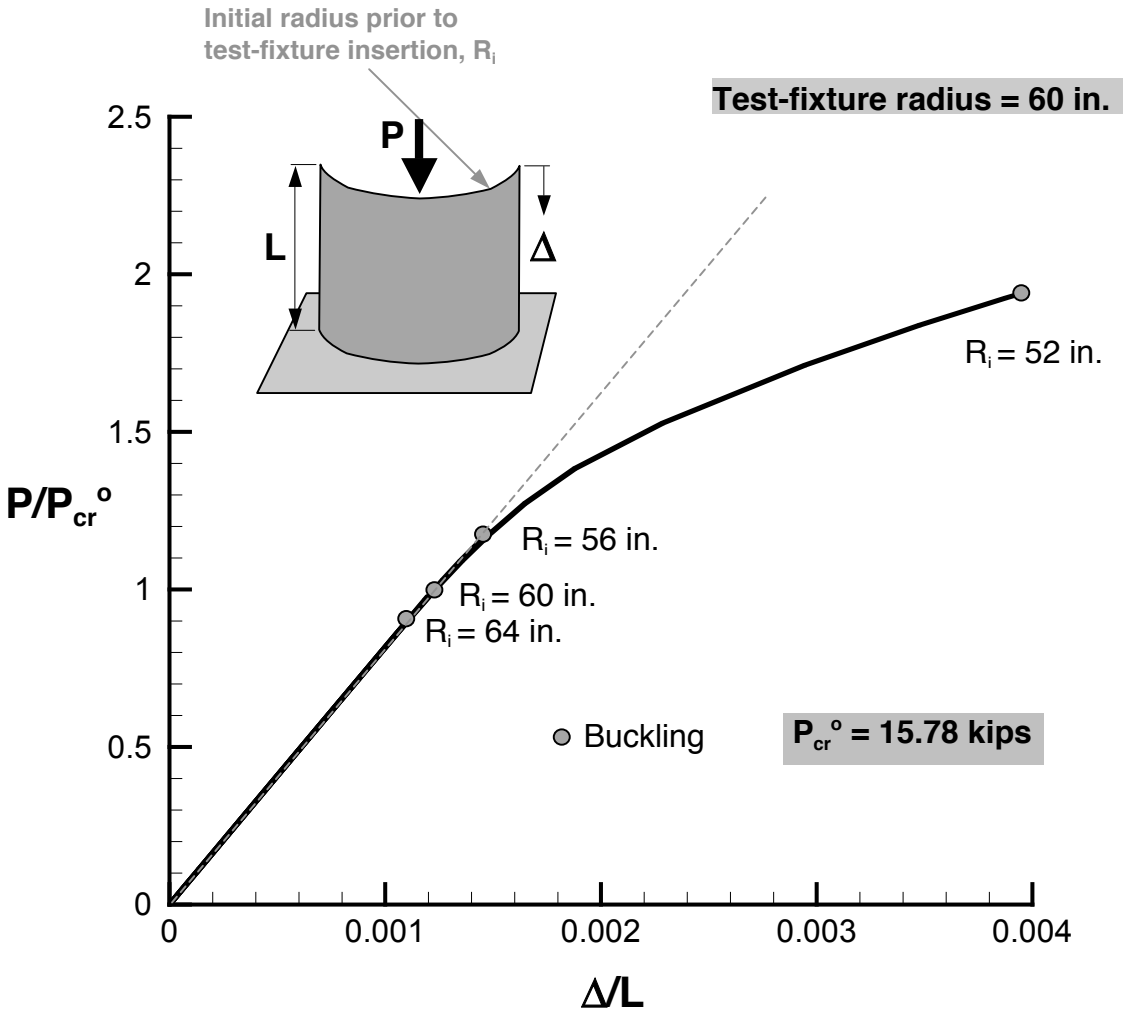

Fig. 13 Effects of prestress on the load-shortening response of compression-loaded, quasi-isotropic curved panels in a 60-in.-radius test fixture.

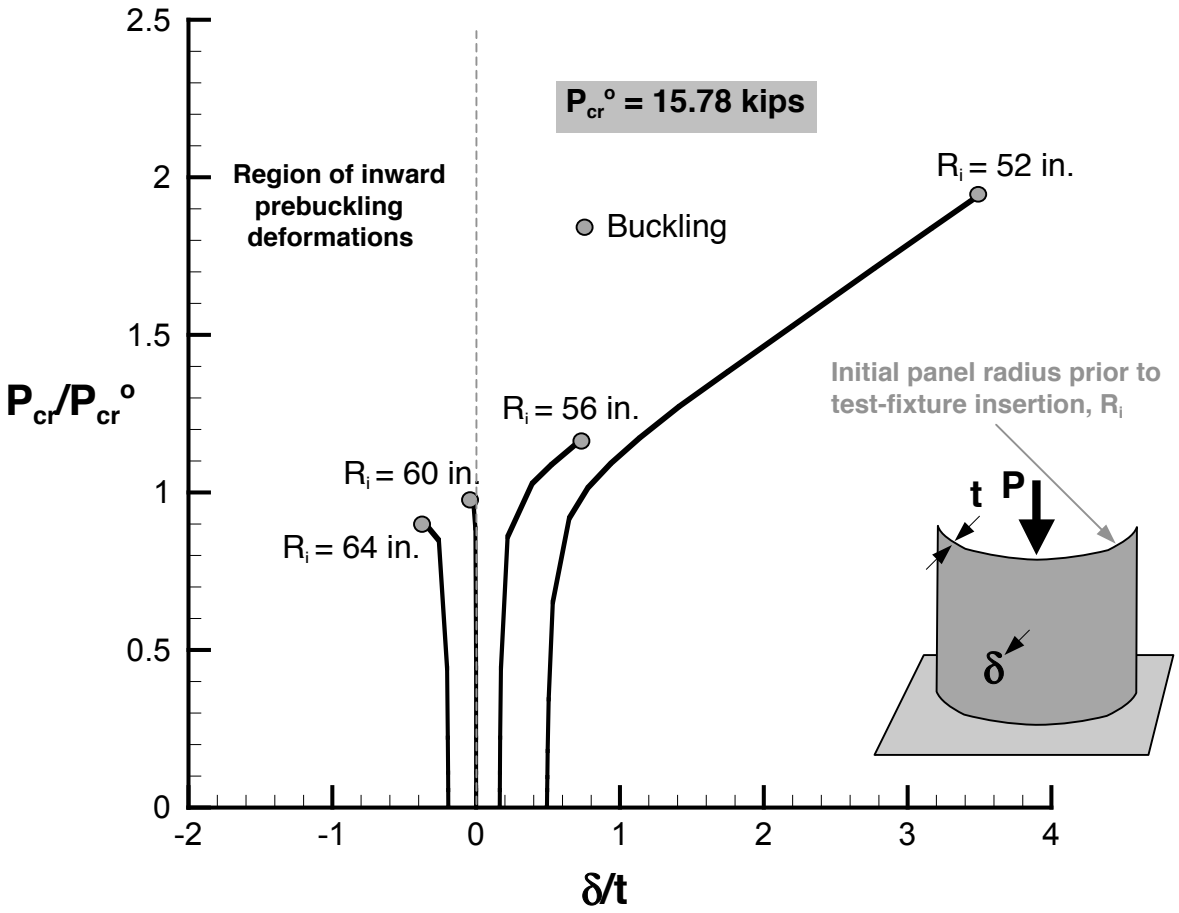

Fig. 14 Effects of prestress on the out-of-plane center displacement of compression-loaded, quasi-isotropic curved panels in a 60-in.-radius test fixture.

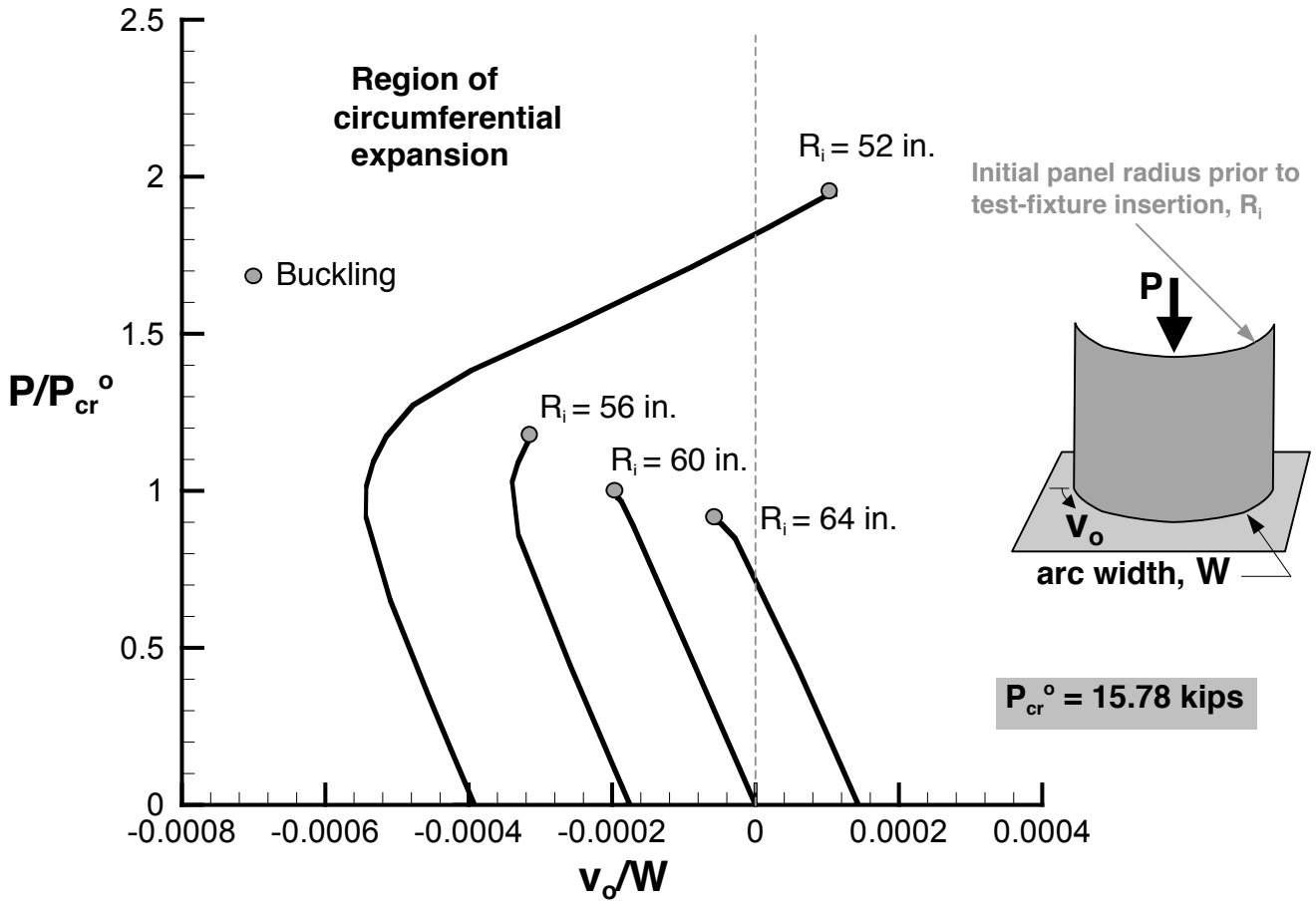

Fig. 15 Effects of prestress on the circumferential displacement response of compression-loaded, quasi-isotropic curved panels in a 60-in.-radius test fixture.

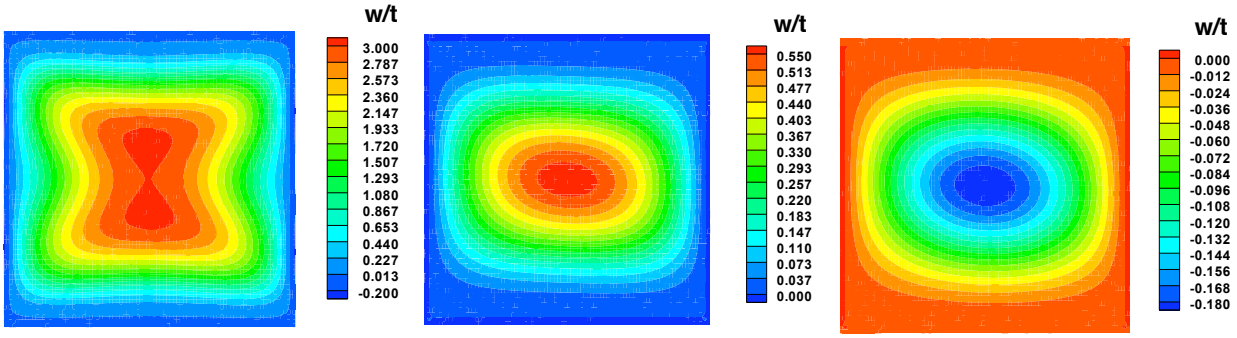

(a) R_i = 52 in., P/P_{cr}^o = 1.94 (b) R_i = 56 in., P/P_{cr}^o = 1.17 (c) R_i = 64 in., P/P_{cr}^o = 0.90

Fig. 16 Effects of prestress on the out-of-plane displacements of compression-loaded, quasi-isotropic curved panels in a 60-in.-radius test fixture.

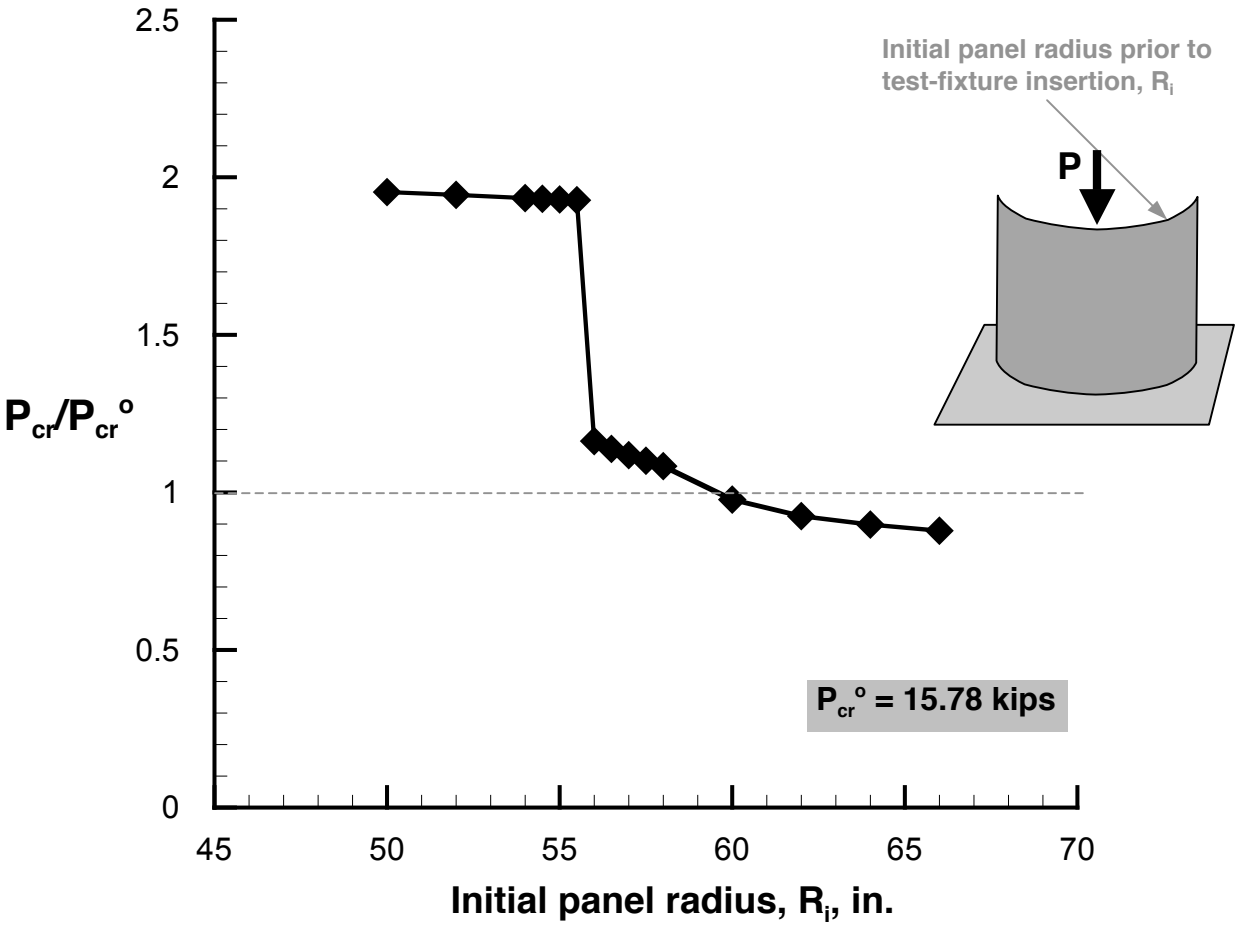

Fig. 17 Effects of prestress on the buckling load of compression-loaded, quasi-isotropic curved panels in a 60-in. radius test fixture.

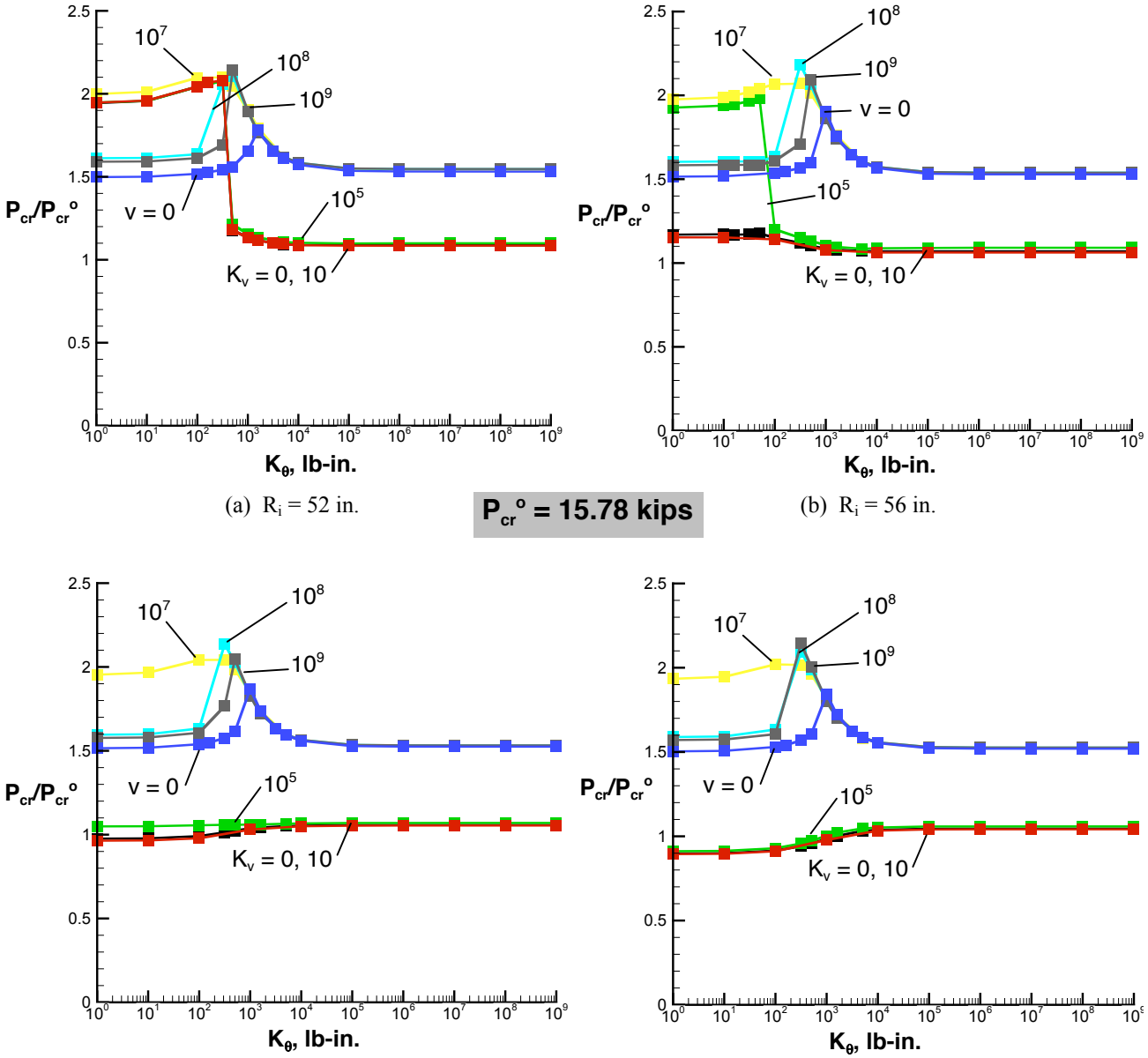

(a) R_i = 52 in.

(b) R_i = 56 in.

(c) R_i = 60 in.

(d) R_i = 64 in.

Fig. 18 Effects of rotational boundary stiffness K_θ, circumferential boundary stiffness K_v, and initial prestress on the buckling load of a compression-loaded, quasi-isotropic, curved panel.

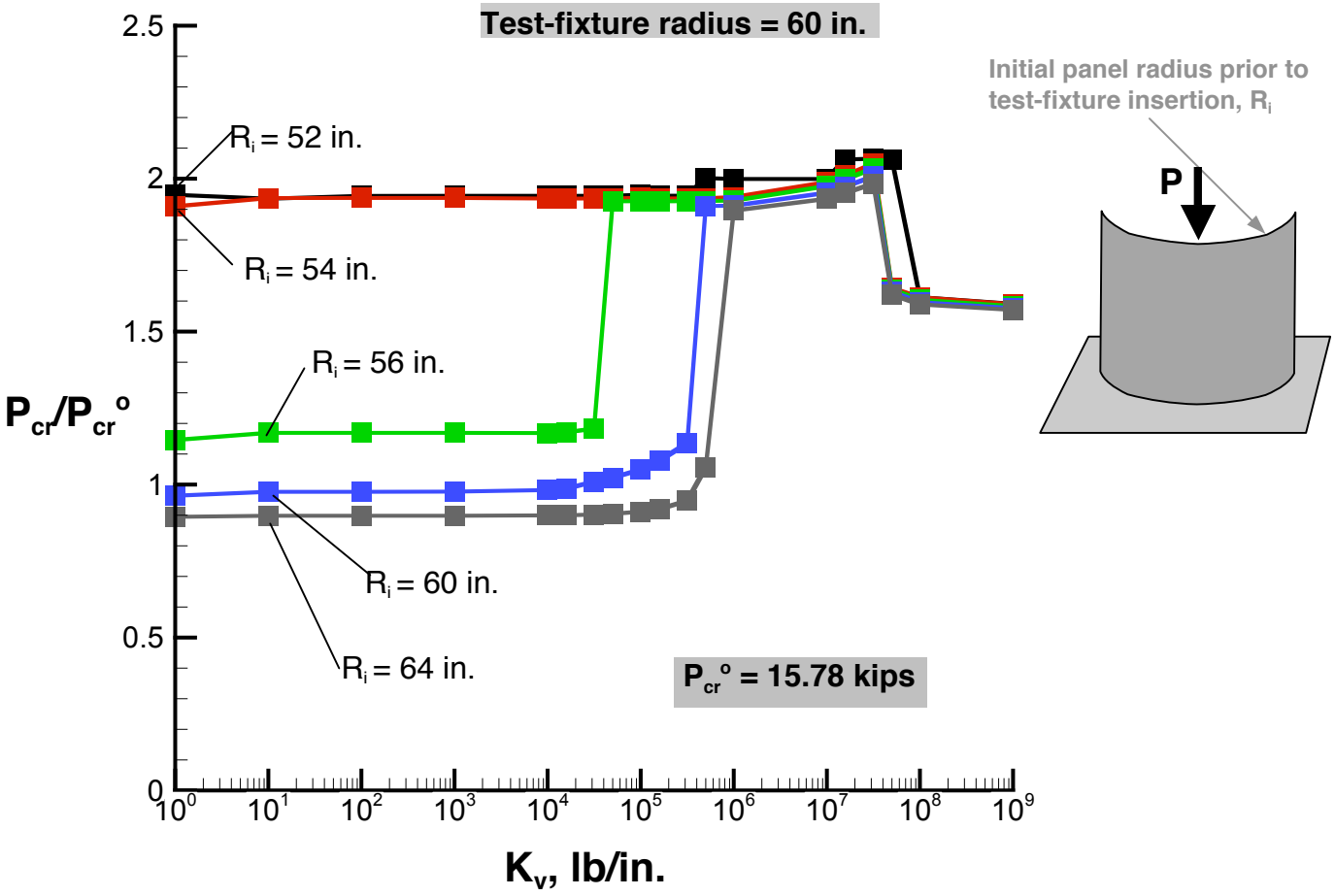

Fig. 19 Effects of initial prestress and circumferential stiffness K_v on the buckling load of compression-loaded, quasi-isotropic, curved panels, $K_\theta = 0$.

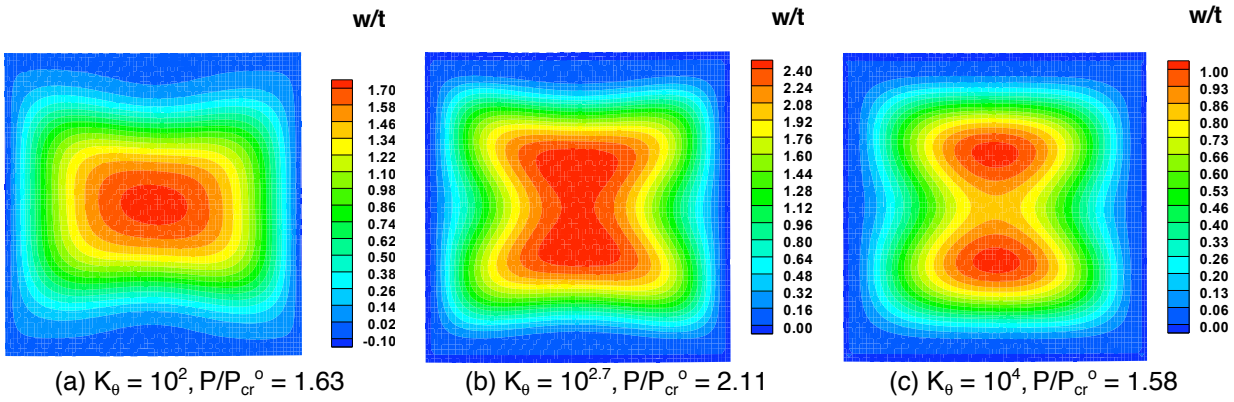

Fig. 20 Combined effects of circumferential boundary stiffness $K_v = 10^8$ lb/in., rotational boundary stiffness K_θ (in.-lb), and prestress on the out-of-plane displacements at the onset of buckling of a 52-in. radius curved panel in a 60-in.-radius test fixture.

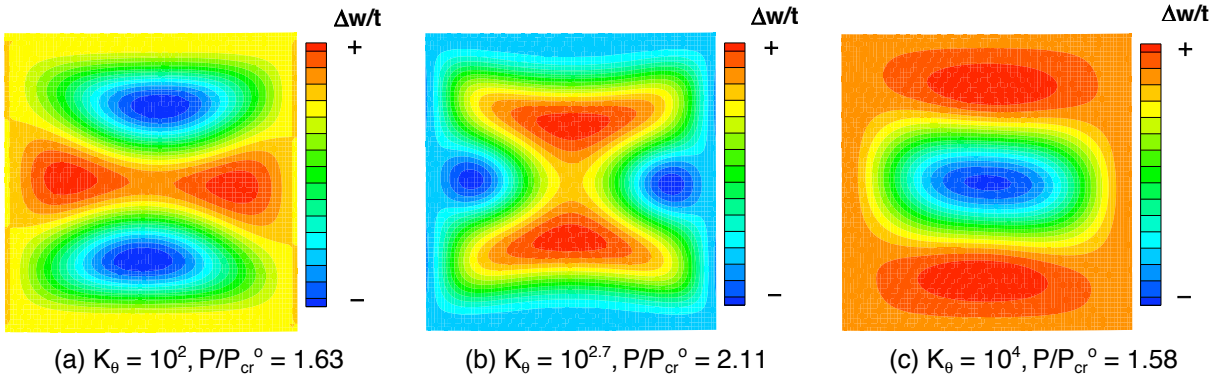

Fig. 21 Combined effects of circumferential boundary stiffness $K_v = 10^8$ lb/in., rotational boundary stiffness K_θ (in.-lb), and prestress the initial out-of-plane displacements at the onset of buckling of a 52-in. radius curved panel in a 60-in.-radius test fixture.